White Rose Research Online

eprints@whiterose.ac.uk
https://eprints.whiterose.ac.uk
Universities of Leeds, Sheffield and York

Deposited via The University of Leeds.

White Rose Research Online URL for this paper:
https://eprints.whiterose.ac.uk/id/eprint/211242/

Version: Accepted Version

Article:
Karageorghis, A. and Lesnic, D. (2025) Solution of the Cauchy problem for the Brinkman equations using an alternating method of fundamental solutions. Numerical Algorithms, 98 (3). pp. 1361-1393. ISSN: 1017-1398

© The Author(s), under exclusive licence to Springer Science+Business Media, LLC, part of Springer Nature 2024. This version of the article has been accepted for publication, after peer review (when applicable) and is subject to Springer Nature's AM terms of use (https://www.springernature.com/gp/open-research/policies/accepted-manuscript-terms), but is not the Version of Record and does not reflect post-acceptance improvements, or any corrections. The Version of Record is available online at: http://dx.doi.org/10.1007/s11075-024-01837-5

Reuse
Items deposited in White Rose Research Online are protected by copyright, with all rights reserved unless indicated otherwise. They may be downloaded and/or printed for private study, or other acts as permitted by national copyright laws. The publisher or other rights holders may allow further reproduction and re-use of the full text version. This is indicated by the licence information on the White Rose Research Online record for the item.

Takedown
If you consider content in White Rose Research Online to be in breach of UK law, please notify us by emailing eprints@whiterose.ac.uk including the URL of the record and the reason for the withdrawal request.

UNIVERSITY OF LEEDS
University of Sheffield
UNIVERSITY of York

SOLUTION OF THE CAUCHY PROBLEM FOR THE BRINKMAN EQUATIONS USING AN ALTERNATING METHOD OF FUNDAMENTAL SOLUTIONS

ANDREAS KARAGEORGHIS AND DANIEL LESNIC

Abstract. In this paper, we intend to formulate and solve Cauchy problems for the Brinkman equations governing the flow of fluids in porous media, which have never been investigated before in such an inverse formulation. The physical scenario corresponds to situations where part of the boundary of the fluid domain is hostile or inaccessible, whilst on the remaining friendly part of the boundary we prescribe or measure both the fluid velocity and traction. The resulting mathematical formulation leads to a linear but ill-posed problem. A convergent algorithm based on solving two sub–sequences of mixed direct problems is developed. The direct solver is based on the method of fundamental solutions which is a meshless boundary collocation method. Since the investigated problem is ill–posed, the iterative process is stopped according to the discrepancy principle at a threshold given by the amount of noise with which the input measured data is contaminated in order to prevent the manifestation of instability. Results inverting both exact and noisy data for two and three-dimensional problems demonstrate the convergence and stability of the proposed numerical algorithm.

1. Introduction

The study of viscous fluid flows is essential when modelling the flow in carbonate reservoirs in petroleum engineering [15] and porous media [3, 4]. Such flows (also called the Stokes resolvent [25]) can be obtained from the unsteady Stokes equations governing the slow viscous flows of incompressible fluids through a Laplace–transform–type procedure. Besides other features, the two–dimensional Brinkman exterior flows do not exhibit a Stokes–like paradox, [18].

In the inverse formulation that we propose – termed the Cauchy problem – one portion of the boundary is accessible and one can prescribe on it both the fluid velocity and traction, while the remaining hostile part of the boundary is inaccessible to inspection or measurement. The unique continuation property of the unsteady Stokes system [5] may be used to establish the uniqueness of solution of this Cauchy problem for the Brinkman system. Other features of the investigation will distinguish between the cases when the over– and under–specified disjoint boundaries are open or closed curves/surfaces. The solution to the linear but ill–posed inverse Cauchy problem will be found by extending the alternating algorithm developed in conjunction with the boundary element

Date: March 31, 2024.
2000 *Mathematics Subject Classification.* Primary 65N35; Secondary 65N21, 65N38.
Key words and phrases. Cauchy problem, inverse problem, Brinkman flow, method of fundamental solutions.

method in [1], where the corresponding Cauchy problem for the Stokes flow was solved. The well–posedness of the mixed problems [12] that need to be solved at each iteration are established in suitable function spaces. Furthermore, recasting the differential boundary value problem (BVP) into an equivalent boundary integral form (based on employing the fundamental solution for the Brinkman system developed in [23]) constitutes an important asset to the analysis and to the numerical implementation based on the method of fundamental solutions (MFS), [11, 24].

The plan of the paper is as follows. The mathematical formulation of the general problem under consideration is given in Section 2, while the definitions and notation employed in the analysis are provided in Section 3. In Section 4 we describe the alternating algorithm to be used for the solution of the Cauchy problem. The unique solvability of the two BVPs involved in the alternating algorithm, as well as a convergence proof of the algorithm are proved in Section 5. In Section 6 a description of the application of the MFS with the proposed algorithm is detailed, and in Section 7 we present some implementational considerations related to the technique. The results of several numerical experiments in two and three dimensions are analysed in Section 8 and, finally, in Section 9 some conclusions and ideas for future work are outlined.

2. Mathematical formulation

The dimensional forms of the Brinkman equations modelling the viscous incompressible fluid flow through a bounded porous medium $\tilde{\Omega} \subset \mathbb{R}^d$, where $d = 2$ or 3, are given by [16]

$$\left\{ \begin{array}{rcl} \mu_e \Delta \tilde{\boldsymbol{u}} - \nabla \tilde{p} - \frac{\tilde{\mu}}{K} \tilde{\boldsymbol{u}} & = & \mathbf{0} \\ \\ \nabla \cdot \tilde{\boldsymbol{u}} = 0 \end{array} \right. \quad \text{in} \quad \tilde{\Omega}, \tag{2.1}$$

where $(\tilde{p}, \tilde{\boldsymbol{u}})$ are the (superficial) pressure and velocity of the fluid flowing through the porous medium, K is the permeability of the porous medium, $\tilde{\mu}$ is the dynamic fluid viscosity and μ_e is the effective (dynamic) viscosity associated with the Brinkman term that is added to the classical Darcy equation to model more accurately fluid flows in highly-porous media. Before performing any analysis all quantities should be non-dimensionalised. Let us introduce the non-dimensional variables

$$\boldsymbol{u} = \tilde{\boldsymbol{u}}/\mathrm{u}_0, \quad \tilde{\boldsymbol{x}} = \tilde{\boldsymbol{x}}/\mathrm{a}, \quad p = \tilde{p}a/(\tilde{\mu}\mathrm{u}_0),$$

where a is a characteristic length dimension of $\tilde{\Omega}$ and u_0 is a characteristic fluid speed. Then, in non-dimensional form the system (2.1) recasts as [11]

$$\left\{ \begin{array}{rcl} \Delta \boldsymbol{u} - \dfrac{1}{\mu} \nabla p - \kappa^2 \boldsymbol{u} & = & \mathbf{0} \\ \\ \nabla \cdot \boldsymbol{u} = 0 \end{array} \right. \quad \text{in} \quad \Omega, \tag{2.2a}$$

where Ω denotes the domain $\tilde{\Omega}$ scaled with its characteristic length dimension a, $\mu = \mu_e/\tilde{\mu}$ is the viscosity ratio and $\kappa^2 = \mathrm{a}^2/(\mu K)$ represents the non-dimensional resitivity of the porous medium. For simplicity, we have assumed that there are no external forces in the system, but a

non–homogeneous known or unknown force term may also be considered in the right–hand side of the first equation of (2.2a), see [19, 20].

In the Cauchy problems analysed in this paper we consider applications in which the boundary $\partial\Omega$ (assumed sufficiently smooth, e.g. of class C^1) consists of a *friendly* portion Γ_0 accessible to measurement whilst the remaining part $\Gamma_1 = \partial\Omega\backslash\Gamma_0$ is *unfriendly* or *hostile* to measurement due to exposure to harsh environmental conditions, e.g. high temperatures/pressures. In such a situation, we prescribe the Cauchy data

$$\boldsymbol{u} = \boldsymbol{\varphi} \quad \text{on} \quad \Gamma_0, \tag{2.2b}$$

and

$$\boldsymbol{t} = \boldsymbol{\psi} \quad \text{on} \quad \Gamma_0, \tag{2.2c}$$

where $\boldsymbol{t}$ represents the non-dimensional fluid traction defined by

$$\boldsymbol{t} = \left(-p\,\mathbf{I} + \mu\left(\nabla\boldsymbol{u} + (\nabla\boldsymbol{u})^{\mathrm{T}}\right)\right)\boldsymbol{n}, \tag{2.3}$$

where $\mathbf{I}$ is the identity tensor and $\boldsymbol{n}$ is the outward unit normal to the boundary $\partial\Omega$. In obtaining (2.3), the dimensional fluid traction defined by

$$\tilde{\boldsymbol{t}} = \left(-\tilde{p}\,\mathbf{I} + \mu_e\left(\nabla\tilde{\boldsymbol{u}} + (\nabla\tilde{\boldsymbol{u}})^{\mathrm{T}}\right)\right)\boldsymbol{n},$$

has been dimensionalised with $\boldsymbol{t} = \tilde{\boldsymbol{t}}\mathrm{a}/(\mathrm{u}_0\tilde{\mu})$. Remark that, from the continuity equation in (2.2a) it follows that $\int_{\partial\Omega}\boldsymbol{u}\cdot\boldsymbol{n}\,dS = 0$, but this condition is not required in the analysis since the Dirichlet velocity data is not prescribed over the whole boundary $\partial\Omega$.

The two possible geometries for the problem under consideration are presented in Figure 1. For the geometry of Figure 1(b), where the sub-boundaries Γ_0 and Γ_1 are closed and disjoint curves, one can extend, in principle, the iterative methods (Landweber, conjugate gradient or minimal error) developed in [8] for the Stokes system. However, if Γ_0 and Γ_1 are open curves with common "corner" points, as in Figure 1(a), one has to modify these iterative methods in appropriately-weighted L^2 spaces, [7], or to apply the alternating algorithm described in Section 4 below.

The above Cauchy problems have been investigated for the scalar Laplace and Helmholtz equations, the vectorial Stokes and Lamé equations, as well as the coupled thermo–elasticity system in references [1, 9, 14, 17] to name only a few, and the purpose of this paper is to extend the inverse analyses for solving the Cauchy problem for the Brinkman system given by (2.2).

3. Definitions and notation

Let Ω be a bounded domain in $\mathbb{R}^d$, with $d = 2$ or 3, with a sufficiently smooth boundary $\partial\Omega$ for the functions defined in the sequel to make sense. Let $H^1(\Omega)$ denote the Sobolev space of functions with the finite norm

$$||u||_{H^1(\Omega)} = \left(\int_\Omega u^2 + \int_\Omega |\nabla u|^2\right)^{1/2}.$$

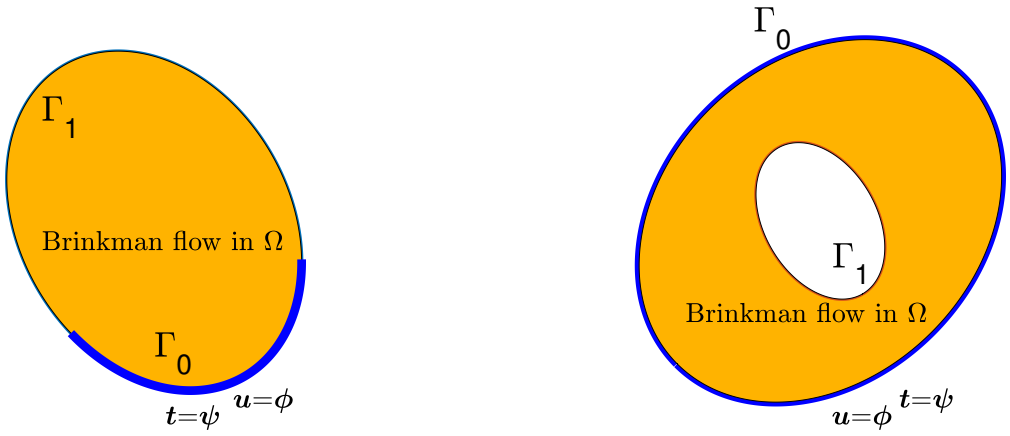

(a) (b)

FIGURE 1. Schematics of the inverse problem under investigation: (a) $\overline{\Gamma}_0 \cap \overline{\Gamma}_1 \neq \emptyset$ and (b) $\overline{\Gamma}_0 \cap \overline{\Gamma}_1 = \emptyset$.

The subspace of functions in $H^1(\Omega)$ which vanish on $\partial\Omega$ is denoted by $H_0^1(\Omega)$. Similarly, we define by $H^1_{\Gamma_i}(\Omega)$ the subspace of functions in $H^1(\Omega)$ vanishing on Γ_i for $i = 0$ or 1. Let $H^{1/2}(\partial\Omega)$ be the space of traces of functions from $H^1(\Omega)$ with the finite norm

$$||u||_{H^{1/2}(\partial\Omega)} = \left(\int_{\partial\Omega} u^2(\boldsymbol{x})\, ds(\boldsymbol{x}) + \int_{\partial\Omega}\int_{\partial\Omega} \frac{|u(\boldsymbol{x}) - u(\boldsymbol{y})|^2}{|\boldsymbol{x}-\boldsymbol{y}|^d}\, ds(\boldsymbol{x})\, ds(\boldsymbol{y}) \right)^{1/2}. \tag{3.1}$$

By replacing $\partial\Omega$ by Γ_i in (3.1), we obtain the spaces $H^{1/2}(\Gamma_i)$ for $i = 0$ or 1. Finally, we define

$$H_{00}^{1/2}(\Gamma_0) := \left\{ u \in H^{1/2}(\partial\Omega) \text{ with } u|_{\Gamma_1} = 0 \right\}$$

with the finite norm

$$||u||_{H_{00}^{1/2}(\Gamma_0)} = \left(\int_{\Gamma_0} \frac{u^2(\boldsymbol{x})}{\operatorname{dist}(\boldsymbol{x}, \Gamma_1)}\, ds(\boldsymbol{x}) + \int_{\Gamma_0}\int_{\Gamma_0} \frac{|u(\boldsymbol{x}) - u(\boldsymbol{y})|^2}{|\boldsymbol{x}-\boldsymbol{y}|^d}\, ds(\boldsymbol{x})\, ds(\boldsymbol{y}) \right)^{1/2}. \tag{3.2}$$

Similarly, one can define $H_{00}^{1/2}(\Gamma_1)$. In what follows, the product of d samples of a space X is denoted by X^d. We also denote by X^* the dual of X.

4. Alternating algorithm

In the iterative alternating algorithm for solving the Cauchy problem (2.2), we employ the following two mixed BVPs:

$$\begin{cases} \Delta \boldsymbol{u} - \dfrac{1}{\mu}\nabla p - \kappa^2 \boldsymbol{u} = \boldsymbol{0} & \text{in} \quad \Omega, \\ \nabla \cdot \boldsymbol{u} = 0 & \text{in} \quad \Omega, \\ \boldsymbol{t} = \boldsymbol{\xi} & \text{on} \quad \Gamma_1, \\ \boldsymbol{u} = \boldsymbol{\varphi} & \text{on} \quad \Gamma_0, \end{cases} \tag{4.1}$$

and

$$\begin{cases} \Delta \boldsymbol{u} - \dfrac{1}{\mu}\nabla p - \kappa^2 \boldsymbol{u} = \boldsymbol{0} & \text{in} \quad \Omega, \\ \nabla \cdot \boldsymbol{u} = 0 & \text{in} \quad \Omega, \\ \boldsymbol{u} = \boldsymbol{\eta} & \text{on} \quad \Gamma_1, \\ \boldsymbol{t} = \boldsymbol{\psi} & \text{on} \quad \Gamma_0, \end{cases} \tag{4.2}$$

where $\boldsymbol{\varphi} \in H^{1/2}(\Gamma_0)^d$ and $\boldsymbol{\psi} \in \left(H_{00}^{1/2}(\Gamma_0)^d\right)^*$ are the same as in (2.2b) and (2.2c), respectively. The alternating algorithm is as follows, (see [1, 2, 9, 14, 22] for Cauchy problems for other elliptic operators):

Algorithm

Step 1: The first approximation $(\boldsymbol{u}_0, p_0)$ is obtained by solving BVP (4.1) with the initial guess $\boldsymbol{\xi} = \boldsymbol{\xi}_0 \in \left(H_{00}^{1/2}(\Gamma_0)^d\right)^*$.

Step 2: Having constructed $(\boldsymbol{u}_{2k}, p_{2k})$, we find $(\boldsymbol{u}_{2k+1}, p_{2k+1})$ by solving BVP (4.2) with $\boldsymbol{\eta} = \boldsymbol{u}_{2k}$ on Γ_1.

Step 3: The next approximation $(\boldsymbol{u}_{2k+2}, p_{2k+2})$ is obtained by solving BVP (4.1) with $\boldsymbol{\xi} = \boldsymbol{t}_{2k+1}$ on Γ_1.

Step 4: The alternating algorithm is continued until a prescribed stopping criterion is satisfied.

5. Theory

In this section, we extend the theory of [1] developed for the stationary Stokes system to the Brinkman system, which differs by the addition of the term $-\kappa^2\boldsymbol{u}$ in the first equation of (2.2a). Although the analysis becomes more involved by the presence of extra terms needed to be considered, the qualitative arguments are actually simpler, e.g., there is no need to employ Korn's inequality, and results slightly stronger, e.g., the operator B defined in (5.32) below is positive in the Brinkman case $\kappa > 0$, see section 5.2.1, whilst in the Stokes case with $\kappa = 0$ the operator B is only non-negative.

We say that $\boldsymbol{u} \in H^1(\Omega)^d$ and $p \in L^2(\Omega)$ form a Brinkman pair if $\nabla \cdot \boldsymbol{u} = 0$ in Ω and

$$\int_\Omega [\boldsymbol{u}, \boldsymbol{v}] - \frac{1}{\mu}\int_\Omega p\, \nabla \cdot \boldsymbol{v} + \kappa^2 \int_\Omega \boldsymbol{u} \cdot \boldsymbol{v} = 0, \quad \forall\, \boldsymbol{v} \in H_0^1(\Omega), \tag{5.1}$$

where

$$\int_\Omega [\boldsymbol{u},\boldsymbol{v}] := \frac{1}{2}\int_\Omega \sum_{i,j=1}^{d}\left(\frac{\partial u_i}{\partial x_j}+\frac{\partial u_j}{\partial x_i}\right)\left(\frac{\partial v_i}{\partial x_j}+\frac{\partial v_j}{\partial x_i}\right). \tag{5.2}$$

Remark that if $(\boldsymbol{u},p)\in H^2(\Omega)^d\times H^1(\Omega)$ is a solution of (2.2a), then it is also a Brinkman pair. Indeed, since $\nabla\cdot\boldsymbol{u}=0$ we can rewrite the first equation in (2.2a) as

$$\sum_{j=1}^{d}\frac{\partial}{\partial x_j}\left(\frac{\partial u_i}{\partial x_j}+\frac{\partial u_j}{\partial x_i}\right)\frac{1}{\mu}\frac{\partial p}{\partial x_i}-\kappa^2 u_i=0 \text{ in } \Omega, \quad i=\overline{1,d}.$$

Multiplying this by $v_i\in H^1(\Omega)$, integrating by parts and summing over i yields

$$\int_{\partial\Omega}\boldsymbol{t}\cdot\boldsymbol{v}=\int_\Omega p\,\nabla\cdot\boldsymbol{v}-\kappa^2\mu\int_\Omega \boldsymbol{u}\cdot\boldsymbol{v}-\mu\int_\Omega[\boldsymbol{u},\boldsymbol{v}], \quad \forall\,\boldsymbol{v}\in H^1(\Omega)^d. \tag{5.3}$$

Thus, if $\boldsymbol{v}\in H_0^1(\Omega)^d$ then $(\boldsymbol{u},p)$ is a Brinkman pair.

Using relation (5.3), we can now define the fluid traction $\boldsymbol{t}$ for an arbitrary Brinkman pair $(\boldsymbol{u},p)\in H^1(\Omega)^d\times L^2(\Omega)$. For this, let us introduce the linear functional on $H^{1/2}(\partial\Omega)^d$ defined by

$$\mathrm{G}(\boldsymbol{\zeta}) := \int_\Omega p\,\nabla\cdot\boldsymbol{v}-\mu\int_\Omega[\boldsymbol{u},\boldsymbol{v}]-\kappa^2\mu\int_\Omega\boldsymbol{u}\cdot\boldsymbol{v}, \tag{5.4}$$

where $\boldsymbol{v}\in H^1(\Omega)^d$ and $\boldsymbol{v}|_{\partial\Omega}=\boldsymbol{\zeta}$. This definition does not depend on $\boldsymbol{v}$ since $(\boldsymbol{u},p)$ is a Brinkman pair. From the definition of the space $H^{1/2}(\partial\Omega)^d$ of traces of functions from $H^1(\Omega)^d$ with the finite norm (3.1), for $\boldsymbol{\zeta}\in H^{1/2}(\partial\Omega)^d$ there exists $\boldsymbol{v}\in H^1(\Omega)^d$ such that $\boldsymbol{v}|_{\partial\Omega}=\boldsymbol{\zeta}$ and $||\boldsymbol{v}||_{H^1(\Omega)^d}\leq c||\boldsymbol{\zeta}||_{H^{1/2}(\partial\Omega)^d}$, where the constant $c\geq 0$ does not depend on $\boldsymbol{\zeta}$. This inequality together with the definition of G in (5.4) yield

$$|\mathrm{G}(\boldsymbol{\zeta})|\leq c_1\left(||\boldsymbol{u}||_{H^1(\Omega)^d}+||p||_{L^2(\Omega)}\right)||\boldsymbol{v}||_{H^1(\Omega)^d}\leq c_2\left(||\boldsymbol{u}||_{H^1(\Omega)^d}+||p||_{L^2(\Omega)}\right)||\boldsymbol{\zeta}||_{H^{1/2}(\partial\Omega)^d}, \tag{5.5}$$

which implies that the functional G is bounded on the space $H^{1/2}(\partial\Omega)^d$. We shall use the notation (2.3) for this functional belonging to $H^{-1/2}(\partial\Omega)^d$. Using the standard continuous extension of the scalar product in $L^2(\partial\Omega)^d$ to $H^{1/2}(\partial\Omega)^d\times H^{-1/2}(\partial\Omega)^d$, we can write the functional (5.4) as

$$\mathrm{G}(\boldsymbol{\zeta})=\int_{\partial\Omega}\boldsymbol{t}\cdot\boldsymbol{\zeta}. \tag{5.6}$$

This extends (5.4) to all Brinkman pairs $(\boldsymbol{u},p)\in H^1(\Omega)^d\times L^2(\Omega)$. The estimate (5.5) implies that

$$||\boldsymbol{t}||_{H^{-1/2}(\partial\Omega)^d}\leq c_2\left(||\boldsymbol{u}||_{H^1(\Omega)^d}+||p||_{L^2(\Omega)}\right). \tag{5.7}$$

The restriction of $\boldsymbol{t}$ to Γ_0, where $(\boldsymbol{u},p)\in H^1(\Omega)^d\times L^2(\Omega)$ is a Brinkman pair, is understood as a functional on $H_{00}^{1/2}(\Gamma_0)^d$, and hence belongs to the space $\left(H_{00}^{1/2}(\Gamma_0)^d\right)^*$.

We now give a condition which guarantees that $\boldsymbol{t}|_{\Gamma_0}\in\left(H^{1/2}(\Gamma_0)^d\right)^*$.

Lemma 1. *Suppose $(\boldsymbol{u},p)\in H^1(\Omega)^d\times L^2(\Omega)$ is a Brinkman pair. If $\boldsymbol{t}|_{\Gamma_1}\in\left(H^{1/2}(\Gamma_1)^d\right)^*$, then $\boldsymbol{t}|_{\Gamma_0}\in\left(H^{1/2}(\Gamma_0)^d\right)^*$.*

Proof. For $\boldsymbol{\zeta} \in H^{1/2}(\Gamma_0)^d$ define the functional

$$\mathrm{F}(\boldsymbol{\zeta}) := \int_\Omega p\, \nabla \cdot \boldsymbol{v} - \mu \int_\Omega [\boldsymbol{u}, \boldsymbol{v}] - \kappa^2 \mu \int_\Omega \boldsymbol{u} \cdot \boldsymbol{v} - \int_{\Gamma_1} \boldsymbol{t} \cdot \boldsymbol{v}, \tag{5.8}$$

where $\boldsymbol{v} \in H^1(\Omega)^d$ and $\boldsymbol{v}|_{\Gamma_0} = \boldsymbol{\zeta}$. According to (5.3), it is enough to prove that (5.8) is well–defined and bounded. For this, first let us choose $\boldsymbol{v}_1, \boldsymbol{v}_2 \in H^1(\Omega)^d$ such that $\boldsymbol{v}_1|_{\Gamma_0} = \boldsymbol{\zeta} = \boldsymbol{v}_2|_{\Gamma_0}$. Then, $(\boldsymbol{v}_1 - \boldsymbol{v}_2)\,|_{\partial\Omega} \in H_{00}^{1/2}(\Gamma_1)^d$. Since $(\boldsymbol{u}, p)$ is a Brinkman pair, from (5.3) we have

$$\int_\Omega p\, \nabla \cdot (\boldsymbol{v}_1 - \boldsymbol{v}_2) - \mu \int_\Omega [\boldsymbol{u}, \boldsymbol{v}_1 - \boldsymbol{v}_2] - \kappa^2 \mu \int_\Omega \boldsymbol{u} \cdot (\boldsymbol{v}_1 - \boldsymbol{v}_2) = \int_{\Gamma_1} \boldsymbol{t} \cdot (\boldsymbol{v}_1 - \boldsymbol{v}_2)\,.$$

Thus, the functional F in (5.8) is well–defined. To show that F is bounded, let $\boldsymbol{v} \in H^1(\Omega)^d$ with $\boldsymbol{v}|_{\Gamma_0} = \boldsymbol{\zeta}$ and $||\boldsymbol{v}||_{H^1(\Omega)^d} \le c||\boldsymbol{\zeta}||_{H^{1/2}(\Gamma_0)^d}$. Then

$$\begin{aligned} |\mathrm{F}(\boldsymbol{\zeta})| &\le c_1 \left(||\boldsymbol{u}||_{H^1(\Omega)^d} + ||p||_{L^2(\Omega)} + ||\boldsymbol{t}||_{\left(H^{1/2}(\Gamma_1)^d\right)^*} \right) ||\boldsymbol{v}||_{H^1(\Omega)^d} \\ &\le c_2 \left(||\boldsymbol{u}||_{H^1(\Omega)^d} + ||p||_{L^2(\Omega)} + ||\boldsymbol{t}||_{\left(H^{1/2}(\Gamma_1)^d\right)^*} \right) ||\boldsymbol{\zeta}||_{H^{1/2}(\Gamma_0)^d}. \end{aligned} \tag{5.9}$$

This implies that the functional F is bounded on $H^{1/2}(\Gamma_0)^d$. If we let $\boldsymbol{\zeta} \in H_{00}^{1/2}(\Gamma_0)^d$, then using (5.3) and (5.8) we obtain that $\mathrm{F} = \boldsymbol{t}|_{\Gamma_0}$, and therefore $\boldsymbol{t}|_{\Gamma_0} \in \left(H^{1/2}(\Gamma_0)^d\right)^*$, which completes the proof of the lemma. □

This lemma enables us to define the weak solution of the Cauchy problem (2.2) with $\boldsymbol{\varphi} \in H^{1/2}(\Gamma_0)^d$ and $\boldsymbol{\psi} \in \left(H_{00}^{1/2}(\Gamma_0)^d\right)^*$, as a Brinkman pair satisfying (2.2b)–(2.2c).

5.1. **Solutions to the mixed direct problems** (4.1) **and** (4.2)**.** Given $\boldsymbol{\eta} \in H^{1/2}(\Gamma_1)^d$ and $\boldsymbol{\psi} \in \left(H_{00}^{1/2}(\Gamma_0)^d\right)^*$, the pair $(\boldsymbol{u}, p) \in H^1(\Omega)^d \times L^2(\Omega)$ is a weak solution of BVP (4.2) if $\nabla \cdot \boldsymbol{u} = 0$ in Ω, $\boldsymbol{u} = \boldsymbol{\eta}$ on Γ_1 and

$$\int_{\Gamma_0} \boldsymbol{\psi} \cdot \boldsymbol{v} = \int_\Omega p\, \nabla \cdot \boldsymbol{v} - \kappa^2 \mu \int_\Omega \boldsymbol{u} \cdot \boldsymbol{v} - \mu \int_\Omega [\boldsymbol{u}, \boldsymbol{v}]\,, \quad \forall\, \boldsymbol{v} \in H^1_{\Gamma_1}(\Omega)^d. \tag{5.10}$$

Notice that a weak solution of BVP (4.2) is a Brinkman pair and that $\boldsymbol{t} = \boldsymbol{\psi}$ on Γ_0. Conversely, if $(\boldsymbol{u}, p)$ is a Brinkman pair with $\boldsymbol{u} = \boldsymbol{\eta} \in H^{1/2}(\Gamma_1)^d$ on Γ_1 and $\boldsymbol{t} = \boldsymbol{\psi} \in \left(H_{00}^{1/2}(\Gamma_0)^d\right)^*$ on Γ_0, then $(\boldsymbol{u}, p)$ is a weak solution to BVP (4.2).

Similarly, letting $\boldsymbol{\varphi} \in H^{1/2}(\Gamma_0)^d$ and $\boldsymbol{\xi} \in \left(H_{00}^{1/2}(\Gamma_1)^d\right)^*$ be given, the pair $(\boldsymbol{u}, p) \in H^1(\Omega)^d \times L^2(\Omega)$ is a weak solution to BVP (4.1) if $\nabla \cdot \boldsymbol{u} = 0$ in Ω, $\boldsymbol{u} = \boldsymbol{\varphi}$ on Γ_0 and

$$\int_{\Gamma_1} \boldsymbol{\xi} \cdot \boldsymbol{v} = \int_\Omega p\, \nabla \cdot \boldsymbol{v} - \kappa^2 \mu \int_\Omega \boldsymbol{u} \cdot \boldsymbol{v} - \mu \int_\Omega [\boldsymbol{u}, \boldsymbol{v}]\,, \quad \forall\, \boldsymbol{v} \in H^1_{\Gamma_0}(\Omega)^d. \tag{5.11}$$

To prove the well–posedness of the direct mixed BVPs (4.1) and (4.2) we also need the following lemma [1, Lemma 5.1].

Lemma 2. *Let $q \in L^2(\Omega)$. Then there exists $\boldsymbol{u} \in H^1_{\Gamma_0}(\Omega)^d$ satisfying*

$$\nabla \cdot \boldsymbol{u} = q \quad in \quad \Omega \tag{5.12}$$

and

$$||\boldsymbol{u}||_{H^1(\Omega)^d} \leq c||q||_{L^2(\Omega)}, \tag{5.13}$$

where the positive constant c is independent of q and $\boldsymbol{u}$.

Theorem 1. *(i) Let $\boldsymbol{\varphi} \in H^{1/2}(\Gamma_0)^d$ and $\boldsymbol{\xi} \in \left(H^{1/2}_{00}(\Gamma_1)^d\right)^*$. Then there exists a unique solution $(\boldsymbol{u}, p) \in H^1(\Omega)^d \times L^2(\Omega)$ to the direct mixed BVP (4.1), which satisfies the stability estimate*

$$||\boldsymbol{u}||_{H^1(\Omega)^d} + ||p||_{L^2(\Omega)} \leq c\left(||\boldsymbol{\varphi}||_{H^{1/2}(\Gamma_0)^d} + ||\boldsymbol{\xi}||_{\left(H^{1/2}_{00}(\Gamma_1)^d\right)^*}\right). \tag{5.14}$$

(ii) Let $\boldsymbol{\eta} \in H^{1/2}(\Gamma_1)^d$ and $\boldsymbol{\psi} \in \left(H^{1/2}_{00}(\Gamma_0)^d\right)^*$. Then there exists a unique solution $(\boldsymbol{u}, p) \in H^1(\Omega)^d \times L^2(\Omega)$ to the direct mixed BVP (4.2), which satisfies the stability estimate

$$||\boldsymbol{u}||_{H^1(\Omega)^d} + ||p||_{L^2(\Omega)} \leq c\left(||\boldsymbol{\eta}||_{H^{1/2}(\Gamma_1)^d} + ||\boldsymbol{\psi}||_{\left(H^{1/2}_{00}(\Gamma_0)^d\right)^*}\right). \tag{5.15}$$

Proof. We only prove (i). Due to the linearity of BVP (4.1), let $(\boldsymbol{u}, p) \in H^1(\Omega)^d \times L^2(\Omega)$ be a solution of it with $\boldsymbol{u} = \boldsymbol{\varphi} = \boldsymbol{0}$ on Γ_0 and $\boldsymbol{t} = \boldsymbol{\xi} = \boldsymbol{0}$ on Γ_1. Then, from the definition (5.11) of a weak solution to BVP (4.1), taking $\boldsymbol{v} = \boldsymbol{u} \in H^1_{\Gamma_0}(\Omega)^d$ and using that $\nabla \cdot \boldsymbol{u} = 0$ in Ω and that $\boldsymbol{t} = \boldsymbol{\xi} = \boldsymbol{0}$ on Γ_1, we obtain

$$\int_\Omega \left\{[\boldsymbol{u}, \boldsymbol{u}] + \kappa^2 |\boldsymbol{u}|^2\right\} = 0. \tag{5.16}$$

This implies that $\boldsymbol{u} = \boldsymbol{0}$ in Ω. Next, since $p \in L^2(\Omega)$, from Lemma 2 there exists $\boldsymbol{v} \in H^1_{\Gamma_0}(\Omega)^d$ satisfying $\nabla \cdot \boldsymbol{v} = p$ in Ω. Using this $\boldsymbol{v}$ in (5.11), we get that $\int_\Omega p^2 = 0$, which implies that $p = 0$ in Ω. Hence, the solution to the mixed BVP (4.1) is unique.

Let us now prove the existence of a solution. Consider first the case when $\boldsymbol{\varphi} = \boldsymbol{0}$ on Γ_0. Then from (5.11), a weak solution $(\boldsymbol{u}, p) \in H^1(\Omega)^d \times L^2(\Omega)$ to BVP (4.1) will satisfy

$$\int_\Omega \left\{[\boldsymbol{u}, \boldsymbol{v}] + \kappa^2 \boldsymbol{u} \cdot \boldsymbol{v}\right\} = -\frac{1}{\mu} \int_{\Gamma_1} \boldsymbol{\xi} \cdot \boldsymbol{v}, \;\; \forall \boldsymbol{v} \in V := \left\{\boldsymbol{v} \in H^1_{\Gamma_0}(\Omega)^d | \nabla \cdot \boldsymbol{v} = 0 \text{ in } \Omega\right\} \text{ and } \boldsymbol{u} \in V. \tag{5.17}$$

Since the right–hand side of (5.17) is a linear bounded functional on the space V, by the Riesz representation theorem it follows that there exists $\boldsymbol{u} \in V$ satisfying (5.17) and

$$||\boldsymbol{u}||_{H^1(\Omega)^d} \leq c||\boldsymbol{\xi}||_{\left(H^{1/2}_{00}(\Gamma_1)^d\right)^*}. \tag{5.18}$$

To show that $p \in L^2(\Omega)$ exists such that relation (5.11) holds, let us define the linear functional $\mathcal{P}$ on $L^2(\Omega)$ by

$$\mathcal{P}(q) := \mu \int_\Omega \left\{[\boldsymbol{u}, \boldsymbol{v}] + \kappa^2 \boldsymbol{u} \cdot \boldsymbol{v}\right\} + \int_{\Gamma_1} \boldsymbol{\xi} \cdot \boldsymbol{v}, \tag{5.19}$$

for every $\boldsymbol{v} \in H^1_{\Gamma_0}(\Omega)^d$ with $\nabla \cdot \boldsymbol{v} = q$ in Ω. This is well–defined since if we take $\boldsymbol{v}_1$, $\boldsymbol{v}_2 \in H^1_{\Gamma_0}(\Omega)^d$ with $\nabla \cdot \boldsymbol{v}_1 = \nabla \cdot \boldsymbol{v}_2$, then

$$\mathcal{P}(\nabla \cdot \boldsymbol{v}_1) - \mathcal{P}(\nabla \cdot \boldsymbol{v}_2) = \mu \int_\Omega \left\{ [\boldsymbol{u}, \boldsymbol{v}_1 - \boldsymbol{v}_1] + \kappa^2 \boldsymbol{u} \cdot (\boldsymbol{v}_1 - \boldsymbol{v}_2) \right\} + \int_{\Gamma_1} \boldsymbol{\xi} \cdot (\boldsymbol{v}_1 - \boldsymbol{v}_2) = 0,$$

where for the last term in the above we have used (5.17) for $\boldsymbol{v} = \boldsymbol{v}_1 - \boldsymbol{v}_2 \in V$. Now, using Lemma 2, for any $q \in L^2(\Omega)$ there exists $\boldsymbol{v} \in H^1_{\Gamma_0}(\Omega)^d$ satisfying $\nabla \cdot \boldsymbol{v} = q$ in Ω and $||\boldsymbol{v}||_{H^1(\Omega)^d} \leq c||q||_{L^2(\Omega)}$, which, based on (5.19), yields the estimate

$$|\mathcal{P}(q)| \leq c_1 \left(||\boldsymbol{u}||_{H^1(\Omega)^d} + ||\boldsymbol{\xi}||_{\left(H^{1/2}_{00}(\Gamma_1)^d\right)^*} \right) ||q||_{L^2(\Omega)}. \tag{5.20}$$

This implies that the linear functional (5.19) is bounded on $L^2(\Omega)$ and by the Riesz representation theorem is follows that there exists $p \in L^2(\Omega)$ such that

$$\int_\Omega p \, \nabla \cdot \boldsymbol{v} = \mu \int_\Omega \left\{ [\boldsymbol{u}, \boldsymbol{v}] + \kappa^2 \boldsymbol{u} \cdot \boldsymbol{v} \right\} + \int_{\Gamma_1} \boldsymbol{\xi} \cdot \boldsymbol{v}, \quad \forall \, \boldsymbol{v} \in H^1_{\Gamma_0}(\Omega)^d, \tag{5.21}$$

which is the definition of the weak solution in (5.11). Hence, in the case $\boldsymbol{\varphi} = \boldsymbol{0}$ we have proved that a solution $(\boldsymbol{u}, p) \in H^1(\Omega)^d \times L^2(\Omega)$ exists. Moreover, from (5.19) and (5.21) we have that $\mathcal{P}(p) = \int_\Omega p^2$ and from (5.20) it follows that

$$||p||_{L^2(\Omega)} \leq c_1 \left(||\boldsymbol{u}||_{H^1(\Omega)^d} + ||\boldsymbol{\xi}||_{\left(H^{1/2}_{00}(\Gamma_1)^d\right)^*} \right). \tag{5.22}$$

Consider now that the Dirichlet data $\boldsymbol{\varphi}$ is arbitrary in $H^{1/2}(\Gamma_0)^d$, and denote by $\tilde{\boldsymbol{\varphi}} \in H^{1/2}(\partial\Omega)^d$ an extension of $\boldsymbol{\varphi}$ to $\partial\Omega$ satisfying

$$\int_{\partial\Omega} \tilde{\boldsymbol{\varphi}} \cdot \boldsymbol{n} = 0 \quad \text{and} \quad ||\tilde{\boldsymbol{\varphi}}||_{H^{1/2}(\partial\Omega)^d} \leq c||\boldsymbol{\varphi}||_{H^{1/2}(\Gamma_0)^d}. \tag{5.23}$$

Then from [21], there exists a unique solution $(\tilde{\boldsymbol{u}}, \tilde{p}) \in H^1(\Omega)^d \times L^2_0(\Omega)$ to the direct Dirichlet problem

$$\left\{ \begin{array}{rcl} \Delta \boldsymbol{u} - \dfrac{1}{\mu} \nabla p - \kappa^2 \boldsymbol{u} = \boldsymbol{0} & \text{in} & \Omega, \\ \nabla \cdot \boldsymbol{u} = 0 & \text{in} & \Omega, \\ \boldsymbol{u} = \tilde{\boldsymbol{\varphi}} & \text{on} & \partial\Omega, \end{array} \right. \tag{5.24}$$

where $L^2_0(\Omega) := \left\{ p \in L^2(\Omega) | \int_\Omega p = 0 \right\} = L^2(\Omega)/\mathbb{R}$. Moreover, from (5.23) and [21]

$$||\tilde{\boldsymbol{u}}||_{H^1(\Omega)^d} + ||\tilde{p}||_{L^2(\Omega)/\mathbb{R}} \leq c_1 ||\tilde{\boldsymbol{\varphi}}||_{H^1(\partial\Omega)^d} \leq c_2 ||\boldsymbol{\varphi}||_{H^{1/2}(\Gamma_0)^d}. \tag{5.25}$$

From the weak solution definition (5.10) or (5.11) applied to the Dirichlet problem (5.24) it follows that $(\tilde{\boldsymbol{u}}, \tilde{p})$ is a Brinkman pair and that $\tilde{\boldsymbol{\xi}} := \tilde{\boldsymbol{t}} \in H^{-1/2}(\partial\Omega)^d$. Then from (5.11) we have

$$\mu \int_\Omega \left\{ [\tilde{\boldsymbol{u}}, \boldsymbol{v}] + \kappa^2 \tilde{\boldsymbol{u}} \cdot \boldsymbol{v} \right\} - \int_\Omega \tilde{p} \, \nabla \cdot \boldsymbol{v} = 0, \quad \forall \, \boldsymbol{v} \in H^1_0(\Omega)^d. \tag{5.26}$$

Also, from (5.11), we have

$$\mu \int_\Omega \left\{ [\tilde{\boldsymbol{u}}, \boldsymbol{v}] + \kappa^2 \tilde{\boldsymbol{u}} \cdot \boldsymbol{v} \right\} - \int_\Omega \tilde{p}\, \nabla \cdot \boldsymbol{v} = - \int_{\Gamma_1} \tilde{\boldsymbol{\xi}} \cdot \boldsymbol{v}, \quad \forall\, \boldsymbol{v} \in (H^1_{\Gamma_0}(\Omega))^d. \tag{5.27}$$

Now let $(\overline{\boldsymbol{u}}, \overline{p}) \in H^1(\Omega)^d \times L^2(\Omega)$ be the weak solution to problem (4.1) with $\overline{\boldsymbol{u}} = \boldsymbol{\varphi} = \boldsymbol{0}$ on Γ_0 and $\overline{\boldsymbol{t}} = \boldsymbol{\xi} - \tilde{\boldsymbol{\xi}}$ on Γ_1, which exists and is unique by the previous arguments. Therefore, from (5.21) it satisfies

$$\int_\Omega \overline{p}\, \nabla \cdot \boldsymbol{v} = \mu \int_\Omega \left\{ [\overline{\boldsymbol{u}}, \boldsymbol{v}] + \kappa^2 \overline{\boldsymbol{u}} \cdot \boldsymbol{v} \right\} + \int_{\Gamma_1} \left(\boldsymbol{\xi} - \tilde{\boldsymbol{\xi}} \right) \cdot \boldsymbol{v}, \quad \forall\, \boldsymbol{v} \in H^1_{\Gamma_0}(\Omega)^d. \tag{5.28}$$

Then, $(\boldsymbol{u}, p) := (\tilde{\boldsymbol{u}}, \tilde{p}) + (\overline{\boldsymbol{u}}, \overline{p})$ is the required solution of BVP (4.1), which satisfies (5.11) by subtracting (5.27) from (5.28). Finally, the stability estimate (5.14) follows from (5.18), (5.22) and (5.25). This concludes the proof of the theorem. □

Before we address the convergence of the alternating procedure described in Section 4, we give a reformulation of the Cauchy problem (2.2).

5.2. **Reformulation of Cauchy problem** (2.2)**.** We introduce the auxiliary operator

$$D_{\Gamma_1} : H^{1/2}(\Gamma_1)^d \to H^1(\Omega)^d \times L^2(\Omega) \ \text{ defined by } \ D_{\Gamma_1} \boldsymbol{\eta} = (\boldsymbol{u}, p)\,, \quad \forall \boldsymbol{\eta} \in H^{1/2}(\Gamma_1), \tag{5.29}$$

where $(\boldsymbol{u}, p)$ solves BVP (4.2) with $\boldsymbol{t} = \boldsymbol{\psi} = \boldsymbol{0}$ on Γ_0, and

$$T_{\Gamma_1} : \left(H^{1/2}_{00}(\Gamma_1)^d \right)^* \to H^1(\Omega)^d \times L^2(\Omega) \ \text{ defined by } \ T_{\Gamma_1} \boldsymbol{\xi} = (\boldsymbol{u}, p)\,, \quad \forall \boldsymbol{\xi} \in \left(H^{1/2}_{00}(\Gamma_1)^d \right)^*, \tag{5.30}$$

where $(\boldsymbol{u}, p)$ solves BVP (4.1) with $\boldsymbol{u} = \boldsymbol{\varphi} = \boldsymbol{0}$ on Γ_0. From (5.14) and (5.15) it follows that the operators D_{Γ_1} and T_{Γ_1} are bounded. Let us also define

$$D_{\Gamma_0} \boldsymbol{\varphi} = (\boldsymbol{u}, p) = \text{ the solution of (4.1) with } \boldsymbol{t} = \boldsymbol{0} \text{ on } \Gamma_1,$$

$$T_{\Gamma_0} \boldsymbol{\psi} = (\boldsymbol{u}, p) = \text{ the solution of (4.2) with } \boldsymbol{u} = \boldsymbol{0} \text{ on } \Gamma_1$$

and

$$\Pi\,(\boldsymbol{u}, p) = \boldsymbol{u}, \ \Lambda_{\Gamma_i} = \boldsymbol{t}|_{\Gamma_i} \text{ and } \Pi_{\Gamma_i}\,(\boldsymbol{u}, p) = \boldsymbol{u}|_{\Gamma_i} \text{ for } i = 0, 1.$$

Now we can reformulate the Cauchy problem (2.2), as follows. Let $\boldsymbol{\xi} \in \left(H^{1/2}_{00}(\Gamma_1)^d \right)^*$ and denote by $(\boldsymbol{u}_0, p_0)$ the solution of BVP (4.1). Clearly, $(\boldsymbol{u}_0, p_0) = T_{\Gamma_1} \boldsymbol{\xi} + D_{\Gamma_0} \boldsymbol{\varphi}$. Now let $(\boldsymbol{u}_1, p_1)$ be the solution of BVP (4.2) with $\boldsymbol{u} = \boldsymbol{\eta} = \boldsymbol{u}_0|_{\Gamma_1}$. Clearly, $(\boldsymbol{u}_1, p_1) = T_{\Gamma_0} \boldsymbol{\psi} + D_{\Gamma_1} \Pi_{\Gamma_1}\,(\boldsymbol{u}_0, p_0)$. It is easy to check that $(\boldsymbol{u}_1, p_1) \in H^1(\Omega)^d \times L^2(\Omega)$ is a solution of (2.2) if and only if $\boldsymbol{\xi}$ satisfies $\Lambda_{\Gamma_1}\,(\boldsymbol{u}_1, p_1) = \boldsymbol{\xi}$. We rewrite this equation as

$$\boldsymbol{\xi} = B\boldsymbol{\xi} + \boldsymbol{h}, \tag{5.31}$$

where

$$B\boldsymbol{\xi} = \Lambda_{\Gamma_1} D_{\Gamma_1} \Pi_{\Gamma_1} T_{\Gamma_1} \boldsymbol{\xi} \quad \text{and} \quad \boldsymbol{h} = \Lambda_{\Gamma_1}\left(D_{\Gamma_1} \Pi_{\Gamma_1} D_{\Gamma_0} \boldsymbol{\varphi} + T_{\Gamma_0} \boldsymbol{\psi} \right). \tag{5.32}$$

Since the operators D_{Γ_1} and T_{Γ_1} are bounded, combined with (5.7) this implies that the operator $B : \left(H^{1/2}_{00}(\Gamma_1)^d \right)^* \to \left(H^{1/2}_{00}(\Gamma_1)^d \right)^*$ is bounded and that $\boldsymbol{h} \in \left(H^{1/2}_{00}(\Gamma_1)^d \right)^*$.

As in [1, Section 7.2], an equivalent norm in $\left(H_{00}^{1/2}(\Gamma_1)^d\right)^*$ is given by

$$||\boldsymbol{\xi}||^2 := \mu \int_\Omega \left\{ [\boldsymbol{u}, \boldsymbol{u}] + \kappa^2 |\boldsymbol{u}|^2 \right\}, \tag{5.33}$$

where $(\boldsymbol{u}, p) = T_{\Gamma_1}\boldsymbol{\xi}$. The corresponding scalar product is defined as

$$\langle \boldsymbol{\xi}, \boldsymbol{\zeta} \rangle := \mu \int_\Omega \left\{ [\boldsymbol{u}, \boldsymbol{v}] + \kappa^2 \boldsymbol{u} \cdot \boldsymbol{v} \right\}, \tag{5.34}$$

where $(\boldsymbol{u}, p) = T_{\Gamma_1}\boldsymbol{\xi}$ and $(\boldsymbol{v}, q) = T_{\Gamma_1}\boldsymbol{\zeta}$.

5.2.1. *Properties of the operator B.* We show that in addition to being linear and bounded, the operator B is also self–adjoint, positive (if $\kappa > 0$), non–expansive and does not have 1 as an eigenvalue. Let $\boldsymbol{\xi} \in \left(H_{00}^{1/2}(\Gamma_1)^d\right)^*$ and denote $(\boldsymbol{v}_0, q_0) = T_{\Gamma_1}\boldsymbol{\xi}$, $(\boldsymbol{v}_1, q_1) = D_{\Gamma_1}(\boldsymbol{v}_0|_{\Gamma_1})$ and $(\boldsymbol{v}_2, q_2) = T_{\Gamma_1}\Lambda_{\Gamma_1}(\boldsymbol{v}_1, q_1)$. Taking another element $\boldsymbol{\zeta} \in \left(H_{00}^{1/2}(\Gamma_1)^d\right)^*$, denote $(\boldsymbol{w}_0, r_0) = T_{\Gamma_1}\boldsymbol{\zeta}$, $(\boldsymbol{w}_1, r_1) = D_{\Gamma_1}\boldsymbol{w}_0|_{\Gamma_1}$ and $(\boldsymbol{w}_2, r_2) = T_{\Gamma_1}\Lambda_{\Gamma_1}(\boldsymbol{w}_1, r_1)$. Then, using the corresponding boundary conditions on $\boldsymbol{v}_2$ and $\boldsymbol{w}_0$ yields

$$\langle B\boldsymbol{\xi}, \boldsymbol{\zeta} \rangle = -\int_{\partial\Omega} \boldsymbol{t}_2(\boldsymbol{v}_2) \cdot \boldsymbol{w}_0 = -\int_{\partial\Omega} \boldsymbol{t}_1(\boldsymbol{v}_1) \cdot \boldsymbol{w}_1 = \mu \int_\Omega \left\{ [\boldsymbol{v}_1, \boldsymbol{w}_1] + \kappa^2 \boldsymbol{v}_1 \cdot \boldsymbol{w}_1 \right\} = \langle \boldsymbol{v}_1, \boldsymbol{w}_1 \rangle.$$

In a similar way, we can obtain that

$$\langle \boldsymbol{\xi}, B\boldsymbol{\zeta} \rangle = -\int_{\partial\Omega} \boldsymbol{t}_2(\boldsymbol{w}_2) \cdot \boldsymbol{v}_0 = -\int_{\partial\Omega} \boldsymbol{t}_1(\boldsymbol{w}_1) \cdot \boldsymbol{v}_1 = \mu \int_\Omega \left\{ [\boldsymbol{w}_1, \boldsymbol{v}_1] + \kappa^2 \boldsymbol{w}_1 \cdot \boldsymbol{v}_1 \right\} = \langle \boldsymbol{w}_1, \boldsymbol{v}_1 \rangle.$$

Hence, the operator B is self–adjoint. To show that B is positive remark that if $0 \not\equiv \boldsymbol{\xi} \in \left(H_{00}^{1/2}(\Gamma_1)^d\right)^*$ then $\boldsymbol{v}_1 \not\equiv 0$ and $\langle B\boldsymbol{\xi}, \boldsymbol{\xi} \rangle = \|\boldsymbol{v}_1\|^2 > 0$. To show that B is non–expansive remark that using (5.33), (5.38) and (5.39) with $\boldsymbol{u}_k = \boldsymbol{v}_k$ for $k = 0, 1, 2$, we obtain

$$||B\boldsymbol{\xi}||^2 = \mu \int_\Omega \left\{ [\boldsymbol{v}_2, \boldsymbol{v}_2] + \kappa^2 |\boldsymbol{v}_2|^2 \right\} \leq \mu \int_\Omega \left\{ [\boldsymbol{v}_0, \boldsymbol{v}_0] + \kappa^2 |\boldsymbol{v}_0|^2 \right\} = ||\boldsymbol{\xi}||^2.$$

Finally, if 1 were an eigenvalue of B, then there would exist $\boldsymbol{0} \neq \boldsymbol{\xi}_0 \in \left(H_{00}^{1/2}(\Gamma_1)^d\right)^*$ such that $B\boldsymbol{\xi}_0 = \boldsymbol{\xi}_0$. This would mean that $\boldsymbol{\xi}_0 = \boldsymbol{t}_2(\boldsymbol{v}_2)|_{\Gamma_1} = \boldsymbol{t}_1(\boldsymbol{v}_1)|_{\Gamma_1}$ and since $\boldsymbol{v}_1|_{\Gamma_1} = \boldsymbol{v}_0|_{\Gamma_1}$ this implies that $(\boldsymbol{v}_1, q_1) = (\boldsymbol{v}_0, q_0)$ because of the same Cauchy data on Γ_1. Furthermore, since $\boldsymbol{v}_0|_{\Gamma_0} = \boldsymbol{0}$ and $\boldsymbol{t}_1(\boldsymbol{v}_1)|_{\Gamma_0} = \boldsymbol{0}$, this implies that $(\boldsymbol{v}_0, q_0) = (\boldsymbol{0}, 0)$ and hence $\boldsymbol{\xi}_0 = \boldsymbol{0}$.

We can now address the convergence of the alternating procedure described in Section 4.

5.3. **Convergence of the alternating procedure.**

Theorem 2. *Let* $\boldsymbol{\varphi} \in H^{1/2}(\Gamma_0)^d$ *and* $\boldsymbol{\psi} \in \left(H_{00}^{1/2}(\Gamma_0)^d\right)^*$. *Assume that the Cauchy problem* (2.2) *has a solution* $(\boldsymbol{u}, p) \in H^1(\Omega)^d \times L^2(\Omega)$. *Let* $(\boldsymbol{u}_{\rm k}, p_{\rm k})$ *be the* k$-th$ *approximate solution in the alternating procedure described in Section 4. Then, for any initial guess* $\boldsymbol{\xi} \in \left(H_{00}^{1/2}(\Gamma_0)^d\right)^*$, *we have that*

$$\lim_{\rm k\to\infty} ||\boldsymbol{u}_{\rm k} - \boldsymbol{u}||_{H^1(\Omega)^d} = 0 \quad \text{and} \quad \lim_{\rm k\to\infty} ||p_{\rm k} - p||_{L^2(\Omega)} = 0. \tag{5.35}$$

Proof. If we start with the initial guess $\boldsymbol{\xi}$ being the exact fluid traction on Γ_1, then we can immediately see that $(\boldsymbol{u}_{\rm k}, p_{\rm k})$ is equal to the exact solution of the Cauchy problem for any ${\rm k} \in \mathbb{N}$. Thus, it is sufficient to prove the convergence relation (5.35) for the trivial solution $(\boldsymbol{u}, p) = (\boldsymbol{0}, 0)$ for zero Cauchy data $\boldsymbol{\varphi} = \boldsymbol{\psi} = \boldsymbol{0}$ on Γ_0. Following the ideas developed in [1, 14], since $\boldsymbol{u}_{\rm k} = \boldsymbol{0}$ or $\boldsymbol{t}_{\rm k} = \boldsymbol{0}$ on Γ_0, from (5.3) we have

$$\mu \int_\Omega \left\{ [\boldsymbol{u}_{\rm k}, \boldsymbol{u}_{\rm k}] + \kappa^2 |\boldsymbol{u}_{\rm k}|^2 \right\} = - \int_{\Gamma_1} \boldsymbol{t}_{\rm k} \cdot \boldsymbol{u}_{\rm k}. \tag{5.36}$$

In the same manner, since $\boldsymbol{u}_{2{\rm k}} = \boldsymbol{0}$ on Γ_0, applying (5.3) with $\boldsymbol{v} = \boldsymbol{u}_{2{\rm k}}$ and $\boldsymbol{u} = \boldsymbol{u}_{2{\rm k}-1}$, we obtain

$$\mu \int_\Omega \left\{ [\boldsymbol{u}_{2{\rm k}-1}, \boldsymbol{u}_{2{\rm k}}] + \kappa^2 \boldsymbol{u}_{2{\rm k}-1} \cdot \boldsymbol{u}_{2{\rm k}} \right\} = - \int_{\Gamma_1} \boldsymbol{t}_{2{\rm k}-1} \cdot \boldsymbol{u}_{2{\rm k}}. \tag{5.37}$$

Also, since $\boldsymbol{t}_{2{\rm k}} = \boldsymbol{t}_{2{\rm k}-1}$ on Γ_1 and using (5.36), from (5.37) we obtain that

$$\mu \int_\Omega \left\{ [\boldsymbol{u}_{2{\rm k}-1}, \boldsymbol{u}_{2{\rm k}}] + \kappa^2 \boldsymbol{u}_{2{\rm k}-1} \cdot \boldsymbol{u}_{2{\rm k}} \right\} = \mu \int_\Omega \left\{ [\boldsymbol{u}_{2{\rm k}}, \boldsymbol{u}_{2{\rm k}}] + \kappa^2 |\boldsymbol{u}_{2{\rm k}}|^2 \right\}.$$

This implies that

$$\begin{aligned} &\int_\Omega \left\{ [\boldsymbol{u}_{2{\rm k}} - \boldsymbol{u}_{2{\rm k}-1}, \boldsymbol{u}_{2{\rm k}} - \boldsymbol{u}_{2{\rm k}-1}] + \kappa^2 |\boldsymbol{u}_{2{\rm k}} - \boldsymbol{u}_{2{\rm k}-1}|^2 \right\} \\ &= \int_\Omega \left\{ [\boldsymbol{u}_{2{\rm k}-1}, \boldsymbol{u}_{2{\rm k}-1}] + \kappa^2 |\boldsymbol{u}_{2{\rm k}-1}|^2 \right\} - \int_\Omega \left\{ [\boldsymbol{u}_{2{\rm k}}, \boldsymbol{u}_{2{\rm k}}] + \kappa^2 |\boldsymbol{u}_{2{\rm k}}|^2 \right\}. \end{aligned} \tag{5.38}$$

Similarly,

$$\begin{aligned} &\int_\Omega \left\{ [\boldsymbol{u}_{2{\rm k}+1} - \boldsymbol{u}_{2{\rm k}}, \boldsymbol{u}_{2{\rm k}+1} - \boldsymbol{u}_{2{\rm k}}] + \kappa^2 |\boldsymbol{u}_{2{\rm k}+1} - \boldsymbol{u}_{2{\rm k}}|^2 \right\} \\ &= \int_\Omega \left\{ [\boldsymbol{u}_{2{\rm k}}, \boldsymbol{u}_{2{\rm k}}] + \kappa^2 |\boldsymbol{u}_{2{\rm k}}|^2 \right\} - \int_\Omega \left\{ [\boldsymbol{u}_{2{\rm k}+1}, \boldsymbol{u}_{2{\rm k}+1}] + \kappa^2 |\boldsymbol{u}_{2{\rm k}+1}|^2 \right\}. \end{aligned} \tag{5.39}$$

One may easily observe that $\boldsymbol{u}_{2{\rm k}} = \boldsymbol{u}_0(B^{\rm k}\boldsymbol{\xi})$ for all ${\rm k} \in \mathbb{N}$, and from the properties of operator B described in Section 5.2.1, we obtain that $\boldsymbol{u}_{2{\rm k}} \to \boldsymbol{0}$ in $H^1(\Omega)^d$. Moreover, relations (5.38) and (5.39) imply that

$$\int_\Omega \left\{ [\boldsymbol{u}_{2{\rm k}-2}, \boldsymbol{u}_{2{\rm k}-2}] + \kappa^2 |\boldsymbol{u}_{2{\rm k}-2}|^2 \right\} \geq \int_\Omega \left\{ [\boldsymbol{u}_{2{\rm k}-1}, \boldsymbol{u}_{2{\rm k}-1}] + \kappa^2 |\boldsymbol{u}_{2{\rm k}-1}|^2 \right\} \geq \int_\Omega \left\{ [\boldsymbol{u}_{2{\rm k}}, \boldsymbol{u}_{2{\rm k}}] + \kappa^2 |\boldsymbol{u}_{2{\rm k}}|^2 \right\},$$

which yields $\boldsymbol{u}_{2{\rm k}-1} \to \boldsymbol{0}$ in $H^1(\Omega)^d$. Overall, we have that $\boldsymbol{u}_{\rm k} \to \boldsymbol{0}$ in $H^1(\Omega)^d$.

To show that $p_{\rm k} \to 0$ in $L^2(\Omega)$, first from Theorem 1(ii), we can estimate the solution $(\boldsymbol{u}_{2{\rm k}+1}, p_{2{\rm k}+1})$ of BVP (4.2) with $\boldsymbol{\psi} = \mathbf{0}$ as, (see (5.15)),

$$||\boldsymbol{u}_{2{\rm k}+1}||_{H^1(\Omega)^d} + ||p_{2{\rm k}+1}||_{L^2(\Omega)} \leq c||\boldsymbol{u}_{2{\rm k}}||_{H^{1/2}(\Gamma_1)^d},$$

which implies that $p_{2{\rm k}+1} \to 0$ in $L^2(\Omega)$. Next, from Theorem 1(i), we may estimate the solution $(\boldsymbol{u}_{2{\rm k}+2}, p_{2{\rm k}+2})$ of BVP (4.1) with $\boldsymbol{\varphi} = \mathbf{0}$ as, (see (5.14)),

$$||\boldsymbol{u}_{2{\rm k}+2}||_{H^1(\Omega)^d} + ||p_{2{\rm k}+2}||_{L^2(\Omega)} \leq c||\boldsymbol{t}_{2{\rm k}+1}||_{\left(H_{00}^{1/2}(\Gamma_1)^d\right)^*}.$$

Observing that

$$\boldsymbol{t}_{2{\rm k}+1} = \left(-p_{2{\rm k}+1}\,\mathbf{I} + \mu\left(\nabla\boldsymbol{u}_{2{\rm k}+1} + (\nabla\boldsymbol{u}_{2{\rm k}+1})^{\rm T}\right)\right)\boldsymbol{n}$$

and using that $p_{2{\rm k}+1} \to 0$ in $L^2(\Omega)$ and $\boldsymbol{u}_{\rm k} \to 0$ in $H^1(\Omega)^d$ it follows that $p_{2{\rm k}} \to 0$ in $L^2(\Omega)$. Thus, overall, $p_{\rm k} \to 0$ in $L^2(\Omega)$ which completes the proof of Theorem 2. □

6. The method of fundamental solutions (MFS)

In two dimensions, we approximate the fluid velocity $\boldsymbol{u} = (u_1, u_2)$ by $\boldsymbol{u}_N = (u_{N_1}, u_{N_2})$, where

$$u_{N_i}(\boldsymbol{x}) = \sum_{j=1}^{N}\left(\alpha_j G_{i1}(\boldsymbol{x}, \boldsymbol{x}'_j) + \beta_j G_{i2}(\boldsymbol{x}, \boldsymbol{x}'_j)\right), \quad i = 1, 2, \quad \boldsymbol{x} \in \overline{\Omega}, \tag{6.1}$$

and the pressure p by p_N where

$$p_N(\boldsymbol{x}) = \sum_{j=1}^{N}\left(\alpha_j P_1(\boldsymbol{x}, \boldsymbol{x}'_j) + \beta_j P_2(\boldsymbol{x}, \boldsymbol{x}'_j)\right), \quad \boldsymbol{x} \in \overline{\Omega}, \tag{6.2}$$

where $\left(\boldsymbol{x}'_j\right)_{j=\overline{1,N}}$ are sources located outside the solution domain $\overline{\Omega}$ and $(G_{ij})_{i,j=1,2}$ and $(P_i)_{i=1,2}$ represent the fundamental solution of the two–dimensional Brinkman and continuity equations (2.2a) given by, see e.g. [11, 23, 24],

$$\begin{aligned} G_{ik}(\boldsymbol{x}, \boldsymbol{x}') = \frac{1}{2\pi\mu\kappa^2 r^2}\Big[&\left(-1 + \kappa r K_1(\kappa r) + \kappa^2 r^2 K_0(\kappa r)\right)\delta_{ik} \\ &+ \frac{(x_i - x'_i)(x_k - x'_k)}{r^2}\left(2 - \kappa^2 r^2 K_2(\kappa r)\right)\Big], \quad i, k = 1, 2, \end{aligned} \tag{6.3}$$

$$P_k(\boldsymbol{x}, \boldsymbol{x}') = \frac{x_k - x'_k}{2\pi r^2}, \quad k = 1, 2, \tag{6.4}$$

where $\boldsymbol{x} = (x_1, x_2)$, $\boldsymbol{x}' = (x'_1, x'_2)$, $r = |\boldsymbol{x} - \boldsymbol{x}'|$, $(\delta_{ik})_{i,k=1,2}$ is the Kronecker delta tensor, and K_n is the modified Bessel function of the second kind of order n.
The fluid traction $\boldsymbol{t} = (t_1, t_2)$ is approximated by $\boldsymbol{t}_N = (t_{N_1}, t_{N_2})$, where

$$t_{N_i}(\boldsymbol{x}) = \sum_{j=1}^{N}\left(\alpha_j D_{i1}(\boldsymbol{x}, \boldsymbol{x}'_j) + \beta_j D_{i2}(\boldsymbol{x}, \boldsymbol{x}'_j)\right), \quad i = 1, 2, \quad \boldsymbol{x} \in \partial\Omega, \tag{6.5}$$

where

$$D_{11} = -P_1\, n_1 + \mu \left(2\, \frac{\partial G_{11}}{\partial x_1}\, n_1 + \left(\frac{\partial G_{21}}{\partial x_1} + \frac{\partial G_{11}}{\partial x_2} \right) n_2 \right),$$
$$D_{12} = -P_2\, n_1 + \mu \left(2\, \frac{\partial G_{12}}{\partial x_1}\, n_1 + \left(\frac{\partial G_{22}}{\partial x_1} + \frac{\partial G_{12}}{\partial x_2} \right) n_2 \right),$$
$$D_{21} = -P_1\, n_2 + \mu \left(\left(\frac{\partial G_{11}}{\partial x_2} + \frac{\partial G_{21}}{\partial x_1} \right) n_1 + 2\, \frac{\partial G_{21}}{\partial x_2}\, n_2 \right),$$
$$D_{22} = -P_2\, n_2 + \mu \left(\left(\frac{\partial G_{12}}{\partial x_2} + \frac{\partial G_{22}}{\partial x_1} \right) n_1 + 2\, \frac{\partial G_{22}}{\partial x_2}\, n_2 \right),$$

where [24]

$$\frac{\partial G_{ik}}{\partial x_j}(\boldsymbol{x}, \boldsymbol{x}') = \frac{1}{2\pi\mu\kappa^2 r^4} \Big\{ (x_j - x_j') \left[2 - \kappa^2 r^2 K_2(\kappa r) - \kappa^3 r^3 K_1(\kappa r) \right] \delta_{ik} + \left((x_k - x_k')\delta_{ij} + (x_i - x_i')\delta_{jk} \right) \left(2 - \kappa^2 r^2 K_2(\kappa r) \right) + \frac{(x_i - x_i')(x_j - x_j')(x_k - x_k')}{r^2} \left[-8 + \kappa^3 r^3 K_3(\kappa r) \right] \Big\}, \quad i, j, k = 1, 2, \tag{6.6}$$

see also [11, Appendix] for alternative forms. The corresponding expressions in three dimensions are provided in the Appendix.

We also place the collocation points $(\boldsymbol{x}_m)_{m=\overline{1,M}}$ on Γ_0 and the collocation points $(\boldsymbol{x}_m)_{m=\overline{M+1,2M}}$ on Γ_1. Collocation of the M boundary conditions for $\boldsymbol{u}$ and $\boldsymbol{t}$ at (alternatively) the M collocation points on Γ_0 and the M collocation points on Γ_1, yields $4M$ equations in the $2N$ unknowns $(\alpha_j)_{j=\overline{1,N}}$ and $(\beta_j)_{j=\overline{1,N}}$. This leads to a system of the form

$$A^{(\mathrm{n})} \left[\frac{\boldsymbol{\alpha}}{\boldsymbol{\beta}} \right] = \boldsymbol{f}^{(\mathrm{n})}, \tag{6.7}$$

where the matrix $A \in \mathbb{R}^{4M \times 2N}$, for $m = \overline{1, M};\ j = \overline{1, N}$, is defined by either

$$A^{(\mathrm{n})}_{m,j} = G_{11}(\boldsymbol{x}_m, \boldsymbol{x}_j'),\ A^{(\mathrm{n})}_{m,N+j} = G_{12}(\boldsymbol{x}_m, \boldsymbol{x}_j'),\ A^{(\mathrm{n})}_{M+m,j} = G_{21}(\boldsymbol{x}_m, \boldsymbol{x}_j'),\ A^{(\mathrm{n})}_{M+m,N+j} = G_{22}(\boldsymbol{x}_m, \boldsymbol{x}_j'),$$
$$A^{(\mathrm{n})}_{2M+m,j} = D_{11}(\boldsymbol{x}_m, \boldsymbol{x}_j'),\ A^{(\mathrm{n})}_{2M+m,N+j} = D_{12}(\boldsymbol{x}_m, \boldsymbol{x}_j'),$$
$$A^{(\mathrm{n})}_{3M+m,j} = D_{21}(\boldsymbol{x}_m, \boldsymbol{x}_j'),\ A^{(\mathrm{n})}_{3M+m,N+j} = D_{22}(\boldsymbol{x}_m, \boldsymbol{x}_j') \quad \text{for} \quad \mathrm{n} = 2\mathrm{k},\ \mathrm{k} \in \mathbb{N}^*,$$

or

$$A^{(\mathrm{n})}_{m,j} = D_{11}(\boldsymbol{x}_m, \boldsymbol{x}_j'),\ A^{(\mathrm{n})}_{m,N+j} = D_{12}(\boldsymbol{x}_m, \boldsymbol{x}_j'),\ A^{(\mathrm{n})}_{M+m,j} = D_{21}(\boldsymbol{x}_m, \boldsymbol{x}_j'),\ A^{(\mathrm{n})}_{M+m,N+j} = D_{22}(\boldsymbol{x}_m, \boldsymbol{x}_j'),$$
$$A^{(\mathrm{n})}_{2M+m,j} = G_{11}(\boldsymbol{x}_m, \boldsymbol{x}_j'),\ A^{(\mathrm{n})}_{2M+m,N+j} = G_{12}(\boldsymbol{x}_m, \boldsymbol{x}_j'),$$
$$A^{(\mathrm{n})}_{3M+m,j} = G_{21}(\boldsymbol{x}_m, \boldsymbol{x}_j'),\ A^{(\mathrm{n})}_{3M+m,N+j} = G_{22}(\boldsymbol{x}_m, \boldsymbol{x}_j') \quad \text{for} \quad \mathrm{n} = 2\mathrm{k}+1,\ \mathrm{k} \in \mathbb{N}.$$

Also, $\boldsymbol{\alpha} = [\alpha_1, \alpha_2, \ldots, \alpha_N]^T$ and $\boldsymbol{\beta} = [\beta_1, \beta_2, \ldots, \beta_N]^T$. Finally,

$$\boldsymbol{f}^{(\mathrm{n})} = \left[\frac{\boldsymbol{\varphi}}{\boldsymbol{\xi}_{\mathrm{n}}} \right] \quad \text{for} \quad \mathrm{n} = 2\mathrm{k},\ \mathrm{k} \in \mathbb{N}^*,$$

or

$$\boldsymbol{f}^{(\mathrm{n})} = \left[\frac{\boldsymbol{\psi}}{\boldsymbol{\eta}_{\mathrm{n}}}\right], \quad \text{for} \quad \mathrm{n} = 2\mathrm{k}+1,\ \mathrm{k} \in \mathbb{N},$$

where, with the notation of the algorithm (with the understanding that $\boldsymbol{t}_0 = \boldsymbol{\xi}_0$) described in Section 4,

$$\boldsymbol{\xi}_{\mathrm{n}} = \boldsymbol{t}_{\mathrm{n}}, \quad \boldsymbol{\eta}_{\mathrm{n}} = \boldsymbol{u}_{\mathrm{n}+1}, \quad \mathrm{n} \in \mathbb{N}.$$

Clearly, in the application of the algorithm, each of the above two matrices only need to be computed once.

7. Implementation details

We consider the two configurations presented in Figure 1.

7.1. **First configuration.** We first examine the case displayed in Figure 1(a). Assuming that the boundary $\partial\Omega$ is a smooth, star–like curve with respect to the origin, in polar coordinates the equation of $\partial\Omega$ is

$$\boldsymbol{x} = (x, y) = r(\vartheta)\ (\cos\vartheta, \sin\vartheta)\,, \qquad \vartheta \in [0, 2\pi), \tag{7.1}$$

where r is a smooth $2\pi-$periodic function. Moreover, let us assume that the portion of the boundary Γ_0 is covered by $0 \le \vartheta \le \Theta$, where $\Theta \in (0, 2\pi)$. We place M collocation points on Γ_0 as follows:

$$\boldsymbol{x}_m = r(\vartheta_m)\ (\cos\vartheta_m, \sin\vartheta_m)\,, \quad \vartheta_m = (m-1)\Theta/(M-1),\ m = \overline{1, M}. \tag{7.2}$$

We also place M collocation points on Γ_1 as follows:

$$\boldsymbol{x}_{M+m} = r(\tilde{\vartheta}_m)\ \left(\cos\tilde{\vartheta}_m, \sin\tilde{\vartheta}_m\right), \quad \tilde{\vartheta}_m = \Theta + m(2\pi - \Theta)/(M+1),\ m = \overline{1, M}. \tag{7.3}$$

Moreover, we take N sources on the pseudo–boundary $\partial\Omega'$ given as

$$\boldsymbol{\xi}_j = \eta\, r(\varphi_j)\ (\cos\varphi_j, \sin\varphi_j)\,, \quad \varphi_j = 2\pi(j-1)/N,\ j = \overline{1, N}, \tag{7.4}$$

where the magnification parameter $\eta > 1$.

In the general case when $\partial\Omega$ does not have a polar representation (7.1), we place $2M$ boundary collocation points $\{\boldsymbol{x}_m\}_{m=1}^{2M}$ on it. We also place the points $\left\{\widetilde{\boldsymbol{\xi}}_j\right\}_{j=1}^{N}$ on $\partial\Omega$ and instead of expression (7.4) for the sources, we take

$$\boldsymbol{\xi}_j = \boldsymbol{x}_{\mathrm{c}} + \eta\,(\widetilde{\boldsymbol{\xi}}_j - \boldsymbol{x}_{\mathrm{c}}) \quad \text{for } j = \overline{1, N}, \tag{7.5}$$

where $\boldsymbol{x}_{\mathrm{c}}$ is the geometric centre of Ω.

7.2. **Second configuration.** We next examine the case displayed in Figure 1(b). We assume that the boundaries Γ_i, $i = 0, 1$, are smooth, star–like curves with respect to the origin with polar equations

$$\boldsymbol{x} = (x, y) = r_i(\vartheta)\ (\cos\vartheta, \sin\vartheta)\,, \qquad \vartheta \in [0, 2\pi), \tag{7.6}$$

where r_i, $i = 0, 1$, are smooth $2\pi-$periodic functions. We place M collocation points on Γ_0 and Γ_1, respectively, as follows:

$$\boldsymbol{x}_m = r_0(\vartheta_m)\ (\cos\vartheta_m, \sin\vartheta_m)\,, \quad \vartheta_m = 2\pi(m-1)/M,\ m = \overline{1, M}, \tag{7.7}$$

and

$$\boldsymbol{x}_{M+m} = r_1(\vartheta_m)\ (\cos\vartheta_m, \sin\vartheta_m)\,, \quad \vartheta_m = 2\pi(m-1)/M,\ m = \overline{1, M}. \tag{7.8}$$

We also take $N/2$ sources on the pseudo–boundaries Γ_0' and Γ_1', respectively, as follows

$$\boldsymbol{\xi}_j = \eta_0\, r_0(\varphi_j)\ (\cos\varphi_j, \sin\varphi_j)\,, \quad \varphi_j = 4\pi(j-1)/N,\ j = \overline{1, N/2}, \tag{7.9}$$

and

$$\boldsymbol{\xi}_{N/2+j} = \eta_1\, r_1(\varphi_j)\ (\cos\varphi_j, \sin\varphi_j)\,, \quad \varphi_j = 4\pi(j-1)/N,\ j = \overline{1, N/2}, \tag{7.10}$$

where the magnification parameter $\eta_0 > 1$ and the contraction parameter $0 < \eta_1 < 1$.

Remarks. In the general case when Γ_0 and Γ_1 do not have a polar representations, arrangements similar to those described in Section 7.1, see (7.5), can be applied for the distribution of the sources. Also, in three dimensions, the curves Γ_0 and Γ_1 replaced by surfaces and the discretization of the boundary $\partial\Omega$ is similar, using spherical coordinates.

7.3. **Stopping criterion.** Instead of the boundary condition (2.2b) we shall consider the noisy data

$$\boldsymbol{\varphi}^{\text{noisy}}(\boldsymbol{x}_m) = (1 + \chi_m \mathrm{p})\, \boldsymbol{\varphi}(\boldsymbol{x}_m), \quad m = \overline{1, M}, \tag{7.11}$$

where $(\chi_m)_{m=\overline{1,M_1}}$ are pseudo–random numbers generated from a uniform distribution in $[-1, 1]$ and p represents the percentage of noise. We stop the iterative process according to the discrepancy principle at the first k for which

$$||\boldsymbol{u}^{2\mathrm{k}} - \boldsymbol{\varphi}^{\text{noisy}}|| \leq ||\boldsymbol{\varphi} - \boldsymbol{\varphi}^{\text{noisy}}||, \tag{7.12}$$

where the fluid velocity solution $\boldsymbol{u}^{2\mathrm{k}} = [u_{N_1}(\boldsymbol{x}_1), \ldots, u_{N_1}(\boldsymbol{x}_M), u_{N_2}(\boldsymbol{x}_1), \ldots, u_{N_2}(\boldsymbol{x}_M)]^T$ is calculated at the k^{th}-iteration.

8. Numerical examples

In all examples considered in this section we took $\mu = 1$ and $\kappa = 2$, while mentioning that numerical results presented in [10] in the case of exterior Brinkman flows did not show significant change in accuracy when these non-dimensional parameters were varied.

8.1. **Example 1.** We consider an annular domain, see Figure 1(b), where $\Omega = \{(x,y)|R_1^2 < x^2+y^2 < R_2^2\}$, with outer boundary Γ_0 the circle of radius R_2, and inner boundary Γ_1 the circle of radius R_1, see [1]. We consider the exact solution which satisfies the Brinkman equations (2.2a), [24],

$$\boldsymbol{u}(x,y) = (\cos(x)\sinh(y), \sin(x)\cosh(y)) \quad \text{and} \quad p(x,y) = -\mu\,\lambda^2\,\sin(x)\sinh(y), \tag{8.1}$$

and select the Cauchy data (2.2b) and (2.2c) for $\boldsymbol{\varphi}$ and $\boldsymbol{\psi}$ on Γ_0 corresponding to this exact solution. We also take $R_1 = 1$, $R_2 = 2$ and choose $\boldsymbol{\xi}_0 = \mathbf{0}$. In the MFS implementation described in Section 7.1, we took $N/2$ sources on an interior circle of radius $3/4$ ($\eta_1 = 3/4$) and $N/2$ sources on an exterior circle of radius $10/3$ ($\eta_0 = 4/3$). Numerical results obtained with $M = 40$ and $N = 60$ are presented and discussed.

In Figure 2 we present the variation of the norm of the error $||\boldsymbol{u} - \boldsymbol{u}^{2k}||$ on the boundary Γ_1 versus the iteration number for no noise in the data (2.2b), i.e. p = 0 in (7.11). From this figure it can be seen that rapid convergence is achieved after only 10 iterations of the alternating algorithm described in Section 4. The corresponding numerical solutions for $\boldsymbol{u} = (u_1, u_2)$, $\boldsymbol{t} = (t_1, t_2)$ and p on Γ_1 obtained after 10 iterations presented in Figure 3 are in excellent agreement with the analytical solutions derived from (8.1) and (2.3).

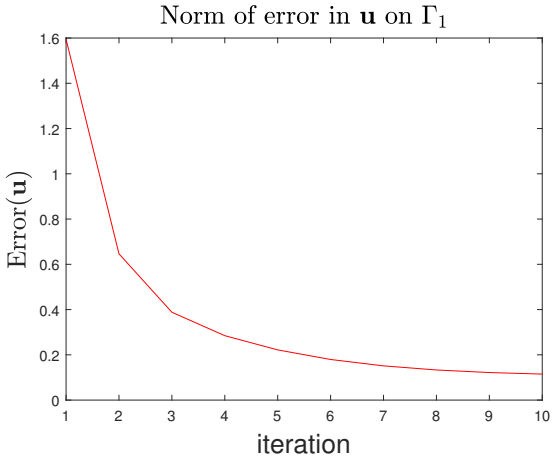

FIGURE 2. Example 1: Variation of the error norm $||\boldsymbol{u} - \boldsymbol{u}^{2k}||$ on Γ_1 with iterations in case of no noise.

Next we investigate the stability of the numerical solution with respect to noise in the fluid velocity data (2.2b), simulated as in (7.11). The variation of the error norm $||\boldsymbol{u}^{2k} - \boldsymbol{\varphi}^{noisy}||$ and the straight line of the norm $||\boldsymbol{\varphi} - \boldsymbol{\varphi}^{noisy}||$ versus the iteration number for noise p = 1%, 3% and 5% are presented in Figure 4. The points where the curves meet the straight lines yield the stopping iteration numbers according to the stopping criterion (7.12). The numerical results for $\boldsymbol{u}$, $\boldsymbol{t}$ and p on Γ_1 obtained by stopping the iterative algorithm at these thresholds presented in Figures 5, 6 and 7 for p = 1%, 3% and 5%, respectively, indicate the stability of the numerical solutions with respect to noise in the input data. From these figures it can also be seen that the

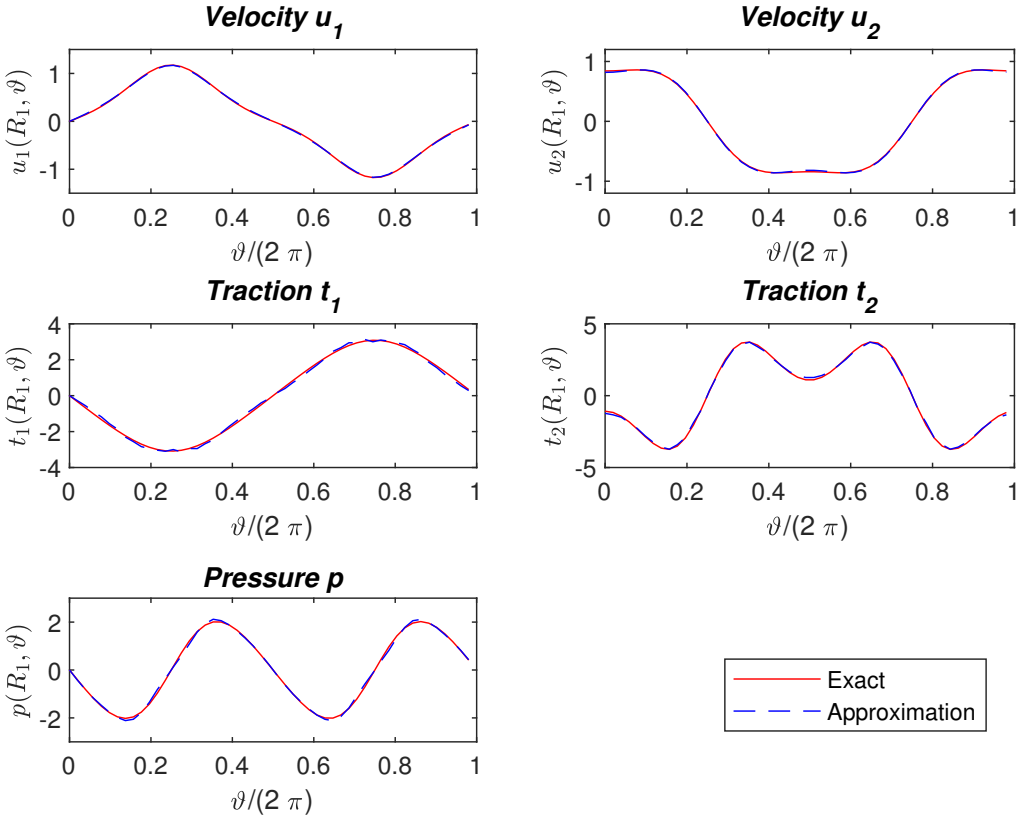

FIGURE 3. Example 1: Results for $\boldsymbol{u}$, $\boldsymbol{t}$ and p on Γ_1, obtained after 10 iterations in case of no noise.

numerical solutions become more accurate as the amount of noise p decreases. The recoveries of the fluid traction and pressure on Γ_1 are less accurate and stable than the fluid velocity because of the derivatives involved, which result in instabilities related to the numerical differentiation of noisy functions.

8.2. **Example 2.** We consider a peanut–shaped domain with the configuration depicted in Figure 1(a), where $r(\vartheta)$ in (7.1) is given by

$$r(\vartheta) = \sqrt{\cos(2\vartheta) + \sqrt{1.1 - \sin^2(2\vartheta)}}, \quad \theta \in [0, 2\pi), \tag{8.2}$$

and the boundary Γ_0 is described by $\Theta = \pi$, see Section 7.1 and Figure 8. Again, we consider the exact solution (8.1), with $\boldsymbol{\xi}_0 = \mathbf{0}$, $\eta = 6$, and present the results obtained with $M = 40$ and $N = 60$.

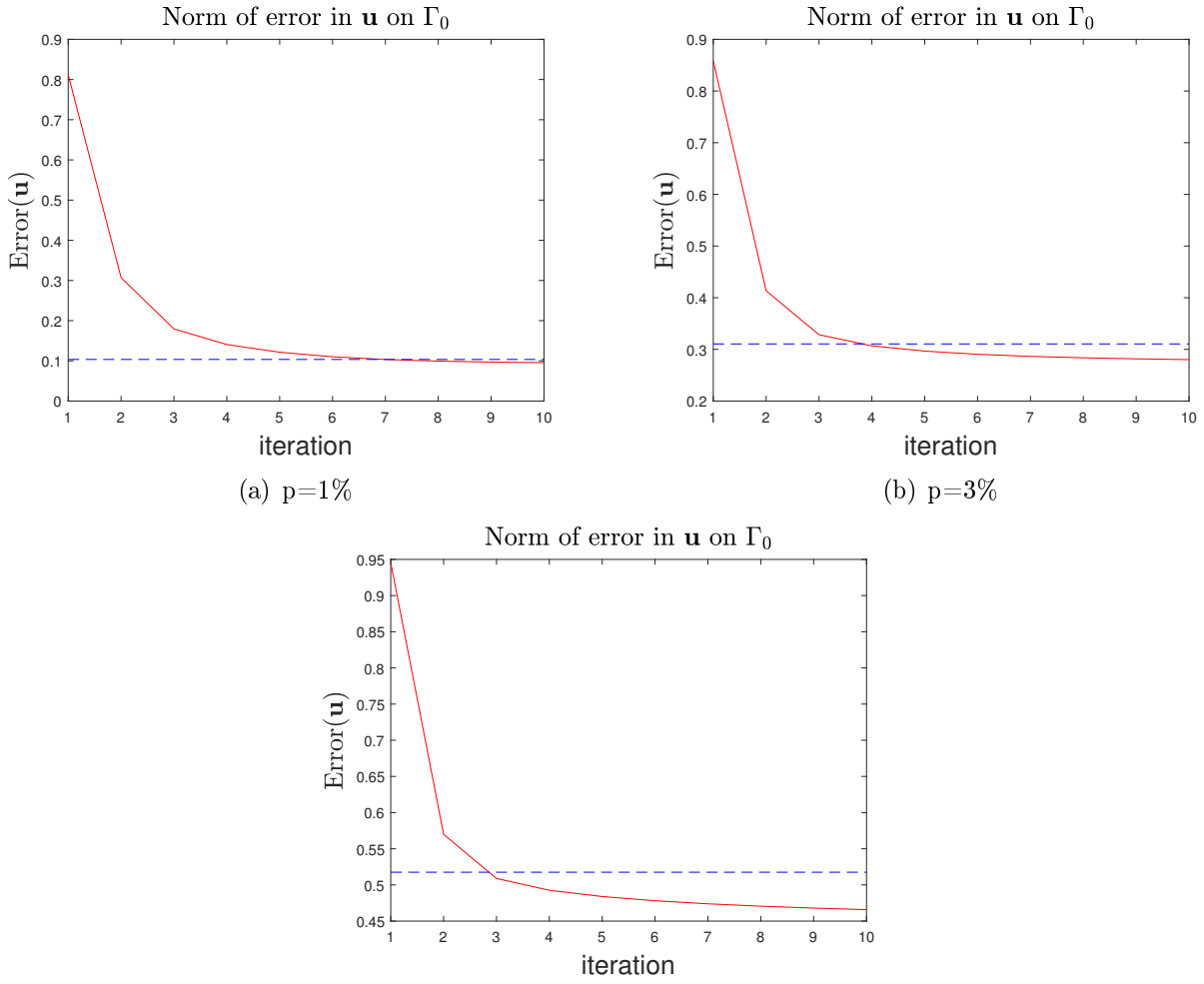

(a) p=1% (b) p=3%

(c) p=5%

FIGURE 4. Example 1: Variation of the error norm $||\boldsymbol{u}^{2k} - \boldsymbol{\varphi}^{noisy}||$ on Γ_0 with iterations for noise p = 1%, 3% and 5%.

The MFS approximations and exact values of $\boldsymbol{u}$, $\boldsymbol{t}$ and p along $\partial\Omega$ obtained after 10000 iterations, no noise, are presented in Figure 9, whilst the results obtained when applying the stopping criterion (7.12) for noise p = 1%, 3% and 5%, are presented in Figures 10, 11 and 12, respectively. The same conclusions as in Example 1 regarding convergence and stability of the numerical solutions can be drawn, although the number of iterations increases significantly in the current example due to the presence of 'corners' where boundaries Γ_0 and Γ_1 meet, which slow down the convergence and affect the accuracy of any numerical scheme.

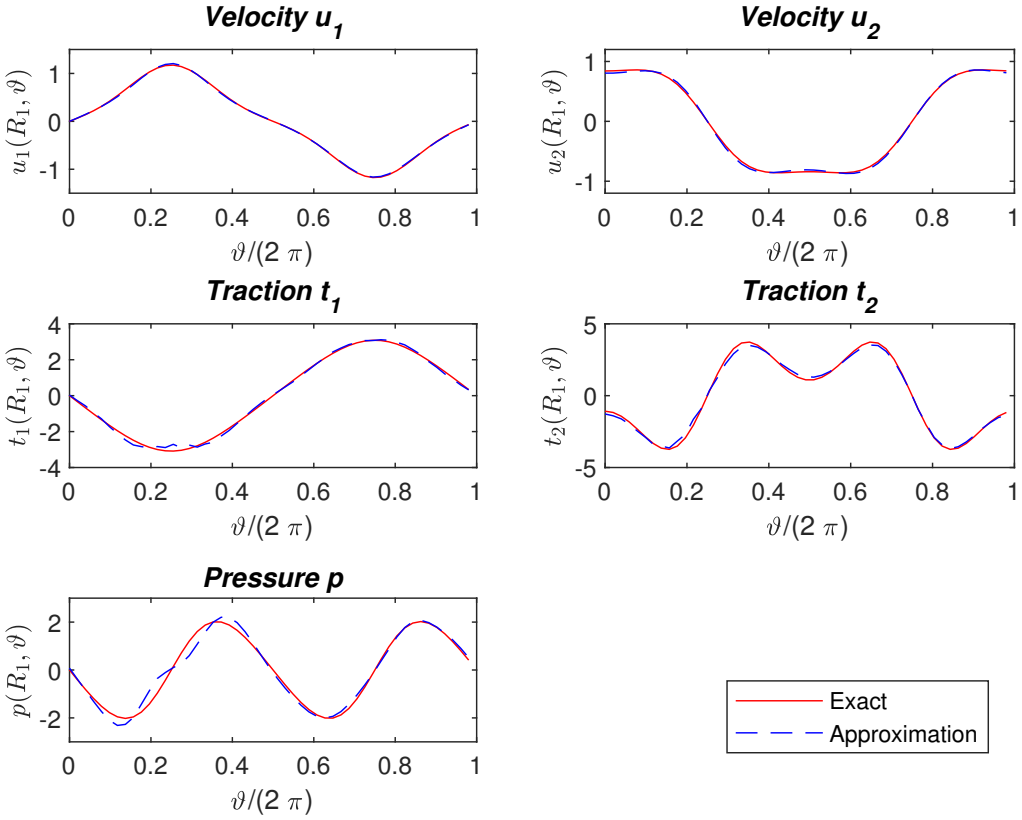

FIGURE 5. Example 1: Results for $\boldsymbol{u}$, $\boldsymbol{t}$ and p on Γ_1, noise p = 1%, obtained after 7 iterations given by the stopping criterion (7.12).

8.3. **Example 3.** We consider a spherical shell $\Omega \subset \mathbb{R}^3$, where $\Omega = \{(x,y,z) | R_1^2 < x^2+y^2+z^2 < R_2^2\}$, with outer boundary Γ_0 the sphere of radius R_2, and inner boundary Γ_1 the sphere of radius R_1. We consider the exact solution which satisfies the three–dimensional Brinkman equations (2.2a), [24],

$$\begin{aligned} \boldsymbol{u}(x,y,z) &= \left(\cos(x)\sinh\left(\frac{y+z}{\sqrt{2}}\right), \sin(x)\cosh\left(\frac{y+z}{\sqrt{2}}\right), \sin(x)\cosh\left(\frac{y+z}{\sqrt{2}}\right)\right), \\ p(x,y,z) &= -\mu\,\lambda^2\,\sin(x)\sinh\left(\frac{y+z}{\sqrt{2}}\right). \end{aligned} \tag{8.3}$$

and take the Cauchy data (2.2b) and (2.2c) for $\boldsymbol{\varphi}$ and $\boldsymbol{\psi}$ on Γ_0 corresponding to this exact solution. We take $R_1 = 1$, $R_2 = 2$ and choose $\boldsymbol{\xi}_0 = \boldsymbol{0}$. In the MFS implementation similar to that described in Section 7.1 for a similar annular geometry to that depicted in Figure 1(a) but

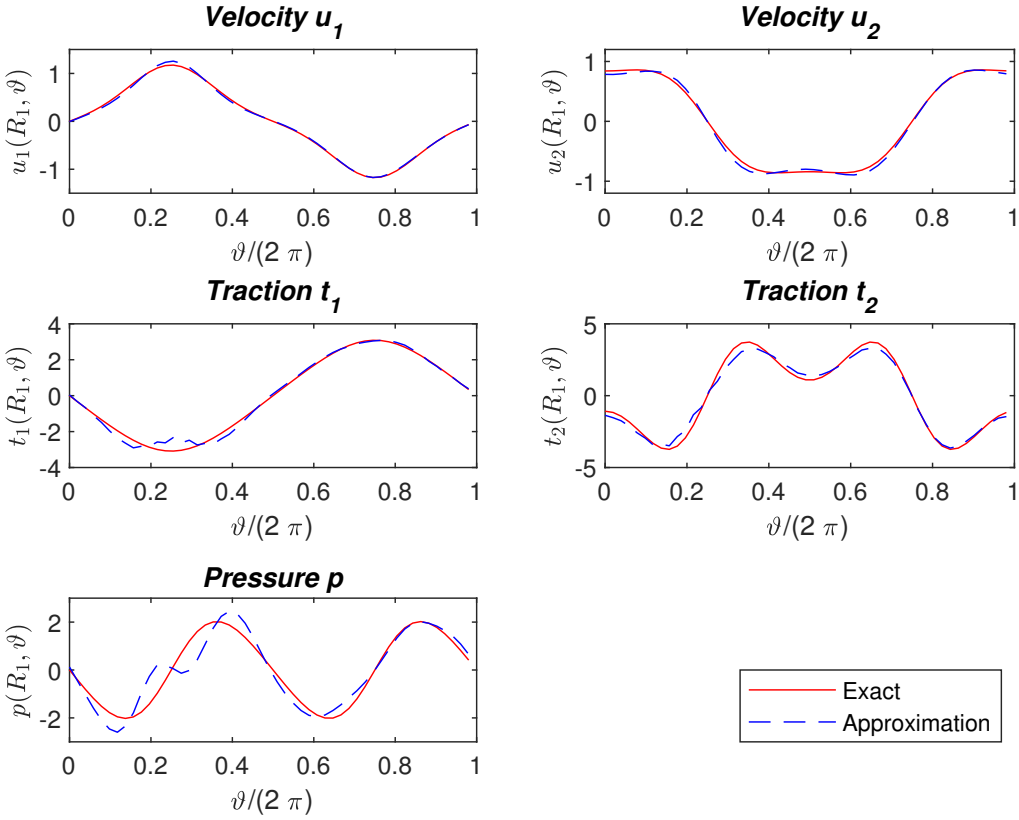

FIGURE 6. Example 1: Results for $\boldsymbol{u}$, $\boldsymbol{t}$ and p on Γ_1, noise p = 3%, obtained after 4 iterations given by the stopping criterion (7.12).

in three-dimensions, i.e. a spherical shell, we took $N/2$ sources on an interior sphere of radius $3/4$ ($\eta_1 = 3/4$) and $N/2$ sources on an exterior sphere of radius 16 ($\eta_0 = 8$).
The collocation points on the unit sphere were distributed as follows. We placed M_2 points on a generating semicircle on the xz-plane with $-\pi/2 < \phi < \phi/2$ avoiding the endpoints, and then we rotated this semicircle about the z-axis with $0 \leq \theta < 2\pi$ producing M_1 points on each circle. The resulting points are thus

$$\boldsymbol{x}_{m,\ell} = (\sin\theta_m \cos\phi_\ell, \cos\theta_m \cos\phi_\ell, \sin\phi_\ell)\,,$$

where $\theta_m = 2\pi(m-1)/M_1,\ m = \overline{1, M_1},\ \phi_\ell = \pi\ell/(M_2+1),\ \ell = \overline{1, M_2}$. The collocation and source points corresponding to each of the four spherical surfaces (two and two, respectively) required in the MFS are generated in this way. A typical such distribution is presented in Figure 13(a). To obtain a more uniform distribution of the boundary collocation points and sources on their respective spherical surfaces, we have also used the so–called Fibonacci sphere algorithm, see,

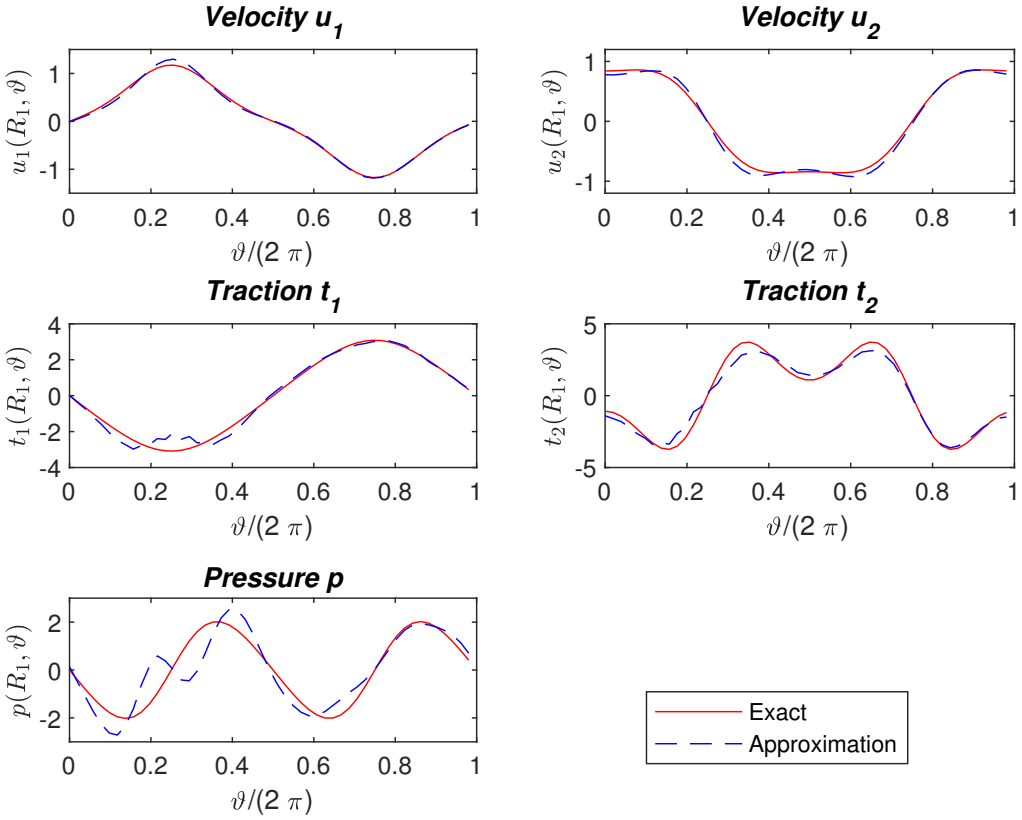

FIGURE 7. Example 1: Results for $\boldsymbol{u}$, $\boldsymbol{t}$ and p on Γ_1, noise p = 5%, obtained after 3 iterations given by the stopping criterion (7.12).

e.g. [6], generating a typical such distribution presented in Figure 13(b). Similar results have been obtained and therefore only the results obtained by the former distribution are illustrated.

The MFS approximations and exact values of $\boldsymbol{u}$, $\boldsymbol{t}$ and p along the circle $x^2 + y^2 = 3/4$ on the surface Γ_1 obtained with $M = 400$, $N = 512$ after 500 iterations, no noise, are presented in Figure 14, whilst the results obtained when applying the stopping criterion (7.12) for noise p = 1%, 3% and 5% are presented in Figures 15, 11 and 17, respectively. The same conclusions as in Example 1 regarding convergence and stability of the numerical solutions can be drawn, although more iterations are required due the increased dimensionality of the problem.

9. CONCLUSIONS

In this paper, ill–posed Cauchy problems for the Brinkman system in isotropic porous media have been solved using an alternating iterative algorithm equipped with an efficient MFS solver. This

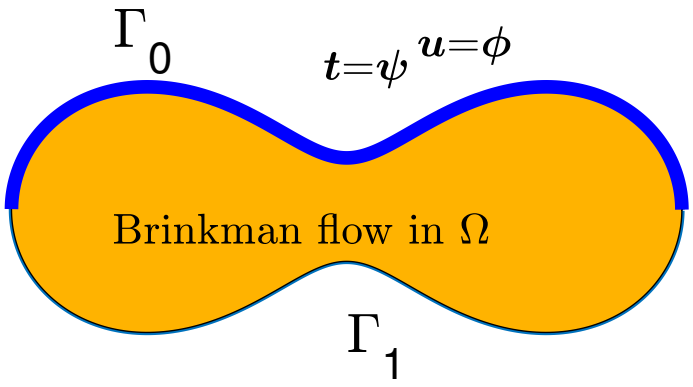

FIGURE 8. Geometry of Example 2.

numerical algorithm was proved to be convergent for exact data and stable (if stopped according to the discrepancy principle) for noisy data. Numerical results obtained for both two- and three-dimensional problems have confirmed the numerical analysis. Future work will deal with extensions associated to the Brinkman equations in anisotropic media [13].

Declarations.
Ethical approval: Not applicable.
Availability of supporting data: Not applicable.
Competing interests: The authors declare no competing interests.
Funding: No funding received.
Authors' contributions: Both authors contributed equally.

Acknowledgments. No data are associated with this article. For the purpose of open access, the authors have applied a Creative Commons Attribution (CC BY) licence to any Author Accepted Manuscript version arising from this submission.

REFERENCES

[1] G. Bastay, B. T. Johansson, V. A. Kozlov and D. Lesnic, *An alternating method for the stationary Stokes system*, ZAMM **86** (2006), 268–280.
[2] J. Baumeister and A. Leitao, *On iterative methods for solving ill–posed problems modeled by partial differential equations*, Journal of Inverse and Ill–Posed Problems **9** (2001), 13–29.
[3] H. C. Brinkman, *A calculation of the viscous force exerted by a flowing fluid is a dense swarm of particles*, Applied Scientific Research **A1** (1949), 27–34.
[4] L. Durlofsky and J. F. Brady, *Analysis of the Brinkman equation as a model for flows in porous media*, Physics of Fluids **30** (1987), 3329–3341.

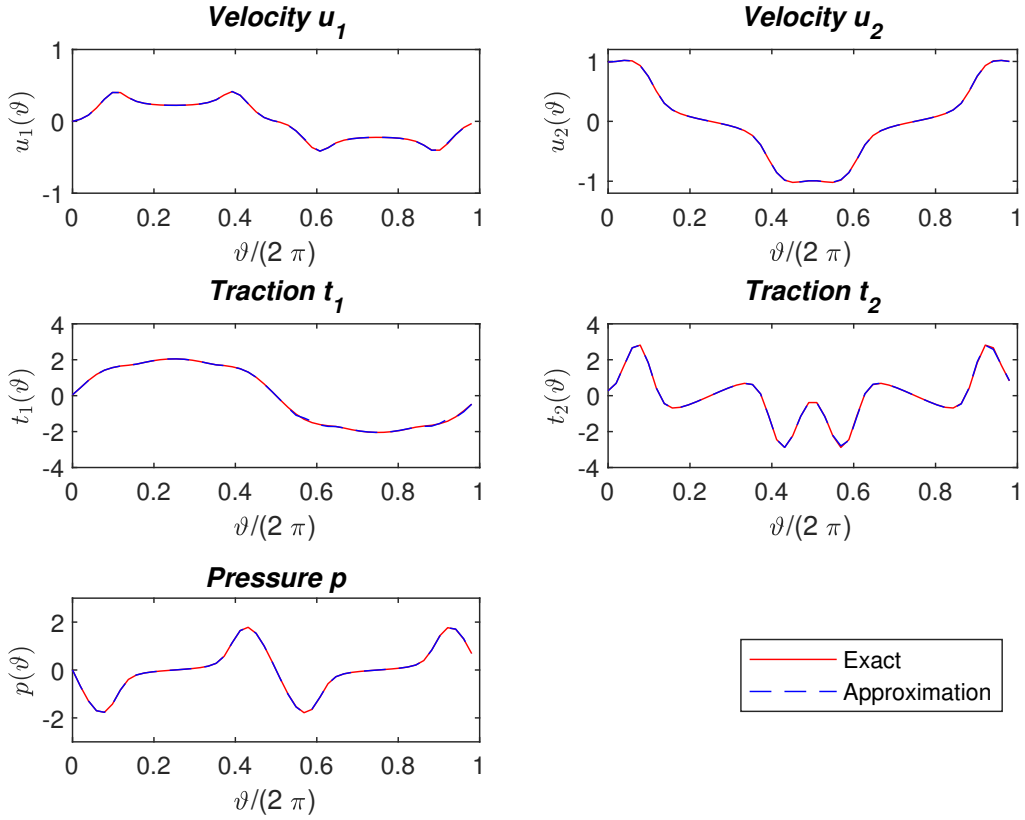

FIGURE 9. Example 2: Results for $\boldsymbol{u}$, $\boldsymbol{t}$ and p on $\partial\Omega$, obtained after 10000 iterations in case of no noise.

[5] C. Fabre and G. Lebeau, *Prolongement unique des solutions de l'equation de Stokes*, Communications in Partial Differential Equations **21** (1996), 573–596.

[6] D. P. Hardin, T. Michaels and E. B. Saff, *A comparison of popular point configurations on* $\mathbb{S}^2$, Dolomites Research Notes on Approximation **9** (2016), 16–49.

[7] T. Johansson, *An iterative procedure for solving a Cauchy problem for second order elliptic equations*, Mathematische Nachrichten **272** (2004), 46–54.

[8] T. Johansson and D. Lesnic, *Reconstruction of a stationary flow from incomplete boundary data using iterative methods*, European Journal of Applied Mathematics **17** (2006), 651–663.

[9] B. T. Johansson and V. A. Kozlov, *An alternating method for Cauchy problems for Helmholtz–type operators in non–homogeneous medium*, IMA Journal of Applied Mathematics **74** (2009), 62–73.

[10] A. Karageorghis, D. Lesnic and L. Marin, *The method of fundamental solutions for Brinkman flows. Part I. Exterior domains*, Journal of Engineering Mathematics **126** (2021), Article number 10, (12 pages).

[11] A. Karageorghis, D. Lesnic and L. Marin, *The method of fundamental solutions for Brinkman flows. Part II. Interior domains*, Journal of Engineering Mathematics **127** (2021), Article number 19, (12 pages).

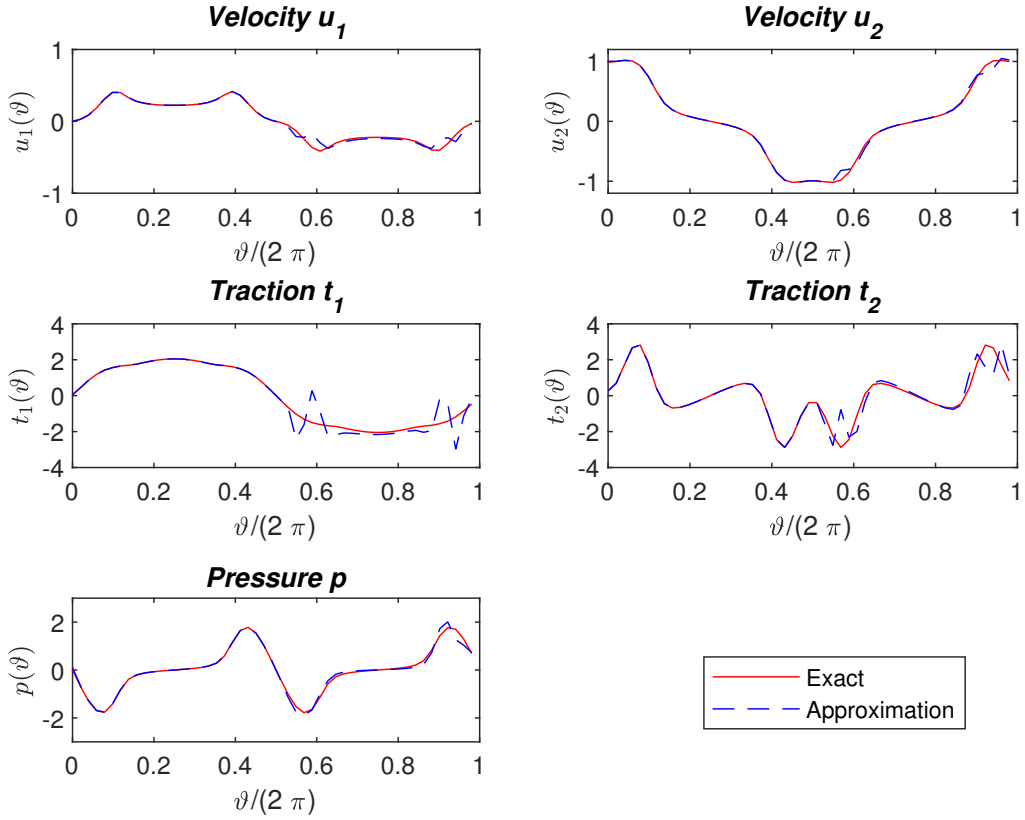

FIGURE 10. Example 2: Results for $\boldsymbol{u}$, $\boldsymbol{t}$ and p on $\partial\Omega$, noise p = 1%, obtained after 723 iterations given by the stopping criterion (7.12).

[12] M. Kohr, *A mixed boundary value problem for the unsteady Stokes system in a bounded domain in* $\mathbb{R}^n$, Engineering Analysis with Boundary Elements **29** (2005), 936–943.

[13] M. Kohr, G. P. Raja Sekhar and J. R. Blake, *Green's function of the Brinkman equation in a 2D anisotropic case*, IMA Journal of Applied Mathematics **73** (2008), 374–392.

[14] V. A. Kozlov, V. G. Maz'ya and A. V. Fomin, *An iterative method for solving the Cauchy problem for elliptic equations*, U.S.S.R. Computational Mathematics and Mathematical Physics **31** (1991), 45–52.

[15] I. S. Ligaarden, M. Krotkiewski, K.-A. Lie, M. Paland and D. W. Schmid, *On the Stokes–Brinkman equations for modelling flow in carbonate reservoirs*, In: Proceedings of the ECMOR XII – 12th European Conference on the Mathematics of Oil Recovery, 6–9 September 2010, Oxford, UK.

[16] H. Liu, P. R. Patil and U. Narusawa, *On Darcy-Brinkman equation: viscous flow between two parallel plates packed with regular square arrays of cylinders*, Entropy **9** (2007), 118–131.

[17] L. Marin, A. Karageorghis and D. Lesnic, *A numerical study of the SVD–MFS solution of inverse boundary problems in two–dimensional steady–state linear thermoelasticity*, Numerical Methods for Partial Differential Equations **31** (2015), 168–201.

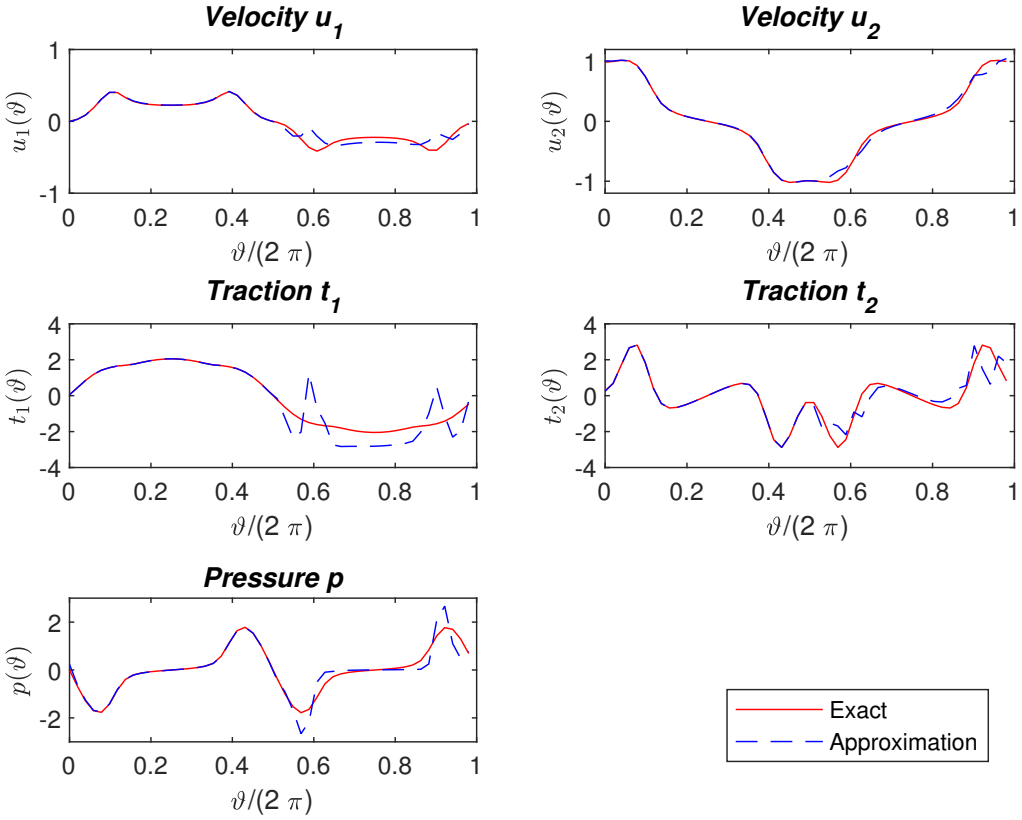

FIGURE 11. Example 2: Results for $\boldsymbol{u}$, $\boldsymbol{t}$ and p on $\partial\Omega$, noise p = 3%, obtained after 153 iterations given by the stopping criterion (7.12).

[18] P. A. Martin, *Two–dimensional Brinkman flows and their relation to analogous Stokes flows*, IMA Journal of Applied Mathematics **84** (2019), 912–929.
[19] N. F. M. Martins and M. Rebelo, *Meshfree methods for non-homogeneous Brinkman flows*, Computers and Mathematics with Applications **68** (2014), 872–886.
[20] N. F. M. Martins, *Identification results for inverse source problems in unsteady Stokes flows*, Inverse Problems **31** (2015), Article 015004, (17pp).
[21] N. F. M. Martins, *Direct and optimization methods for the localization of obstacles in porous media*, in Engineering Optimization IV (eds. H. Rodrigues et al.), Taylor & Francis Group, London, 2015, pp. 991–996.
[22] D. Maxwell, *Kozlov–Maz'ya iteration as a form of Landweber iteration*, Inverse Problems and Imaging **8** (2014), 537–560.
[23] C. Pozrikidis, *Boundary Integral and Singularity Methods for Linearized Viscous Flow*, Cambridge University Press, Cambridge, 1992.
[24] C. C. Tsai, *Solutions of slow Brinkman flows using the method of fundamental solutions*, International Journal for Numerical Methods in Fluids **56** (2008), 927–940.

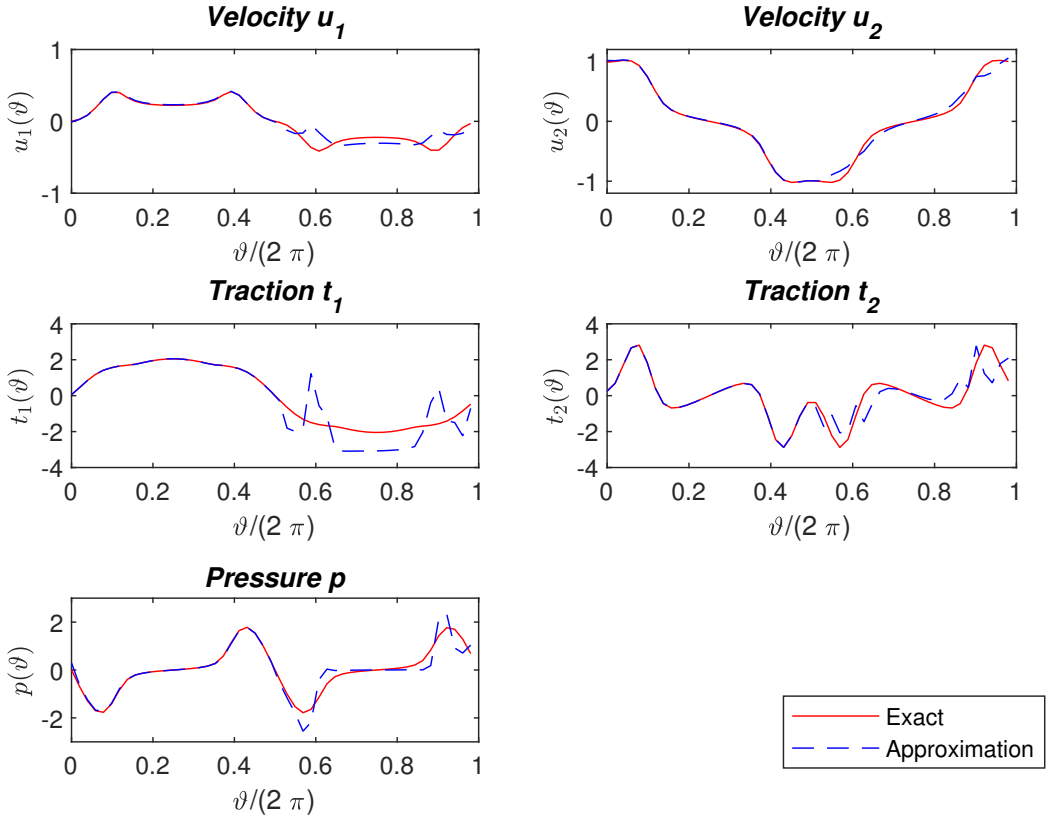

FIGURE 12. Example 2: Results for $\boldsymbol{u}$, $\boldsymbol{t}$ and p on $\partial\Omega$, noise p = 5%, obtained after 67 iterations given by the stopping criterion (7.12).

[25] W. Varnhorn, *The boundary value problems of the Stokes resolvent equations in n dimensions*, Mathematische Nachrichten **267-270** (2004), 210–230.

APPENDIX

In three dimensions, we approximate the fluid velocity $\boldsymbol{u} = (u_1, u_2, u_3)$ and the pressure p by $\boldsymbol{u}_N = (u_{N_1}, u_{N_2}, u_{N_3})$ and p_N, respectively, where

$$u_{N_i}(\boldsymbol{x}) = \sum_{j=1}^{N} \left(\alpha_j G_{i1}(\boldsymbol{x}, \boldsymbol{x}'_j) + \beta_j G_{i2}(\boldsymbol{x}, \boldsymbol{x}'_j) + \gamma_j G_{i3}(\boldsymbol{x}, \boldsymbol{x}'_j)\right), \quad i = 1, 2, 3, \quad \boldsymbol{x} \in \overline{\Omega}, \tag{A.1}$$

(a) (b)

FIGURE 13. Typical node distributions on sphere.

and the pressure p by p_N where

$$p_N(\boldsymbol{x}) = \sum_{j=1}^{N} \left(\alpha_j P_1(\boldsymbol{x}, \boldsymbol{x}'_j) + \beta_j P_2(\boldsymbol{x}, \boldsymbol{x}'_j) + \gamma_j P_3(\boldsymbol{x}, \boldsymbol{x}'_j)\right), \quad \boldsymbol{x} \in \overline{\Omega}, \tag{A.2}$$

where

$$G_{ik}(\boldsymbol{x}, \boldsymbol{x}') = \frac{1}{4\pi\mu\kappa^2 r^3}\left[\left(-1 + \left(1 + \kappa r + \kappa^2 r^2\right)\mathrm{e}^{-\kappa r}\right)\delta_{ik} + \frac{(x_i - x'_i)(x_k - x'_k)}{r^2}\left(3 - \left(3 + 3\kappa r + \kappa^2 r^2\right)\mathrm{e}^{-\kappa r}\right)\right], \quad i, k = 1, 2, 3, \tag{A.3}$$

$$P_k(\boldsymbol{x}, \boldsymbol{x}') = \frac{x_k - x'_k}{4\pi r^3}, \quad k = 1, 2, 3, \tag{A.4}$$

is the fundamental solution of the three–dimensional Brinkman and continuity equations (2.2a), see e.g. [23, 24]. The approximation for the fluid traction $\boldsymbol{t} = (t_1, t_2, t_3)$ is $\boldsymbol{t}_N = (t_{N_1}, t_{N_2}, t_{N_3})$, where

$$t_{N_i}(\boldsymbol{x}) = \sum_{j=1}^{N} \left(\alpha_j D_{i1}(\boldsymbol{x}, \boldsymbol{x}'_j) + \beta_j D_{i2}(\boldsymbol{x}, \boldsymbol{x}'_j) + \gamma_j D_{i3}(\boldsymbol{x}, \boldsymbol{x}'_j)\right), \quad i = 1, 2, 3, \quad \boldsymbol{x} \in \partial\Omega, \tag{A.5}$$

with

$$D_{i\ell} = -P_\ell\, n_i + \mu \sum_{k=1}^{3} \left(\frac{\partial G_{i\ell}}{\partial x_k} + \frac{\partial G_{k\ell}}{\partial x_i}\right) n_k, \quad i, \ell = 1, 2, 3. \tag{A.6}$$

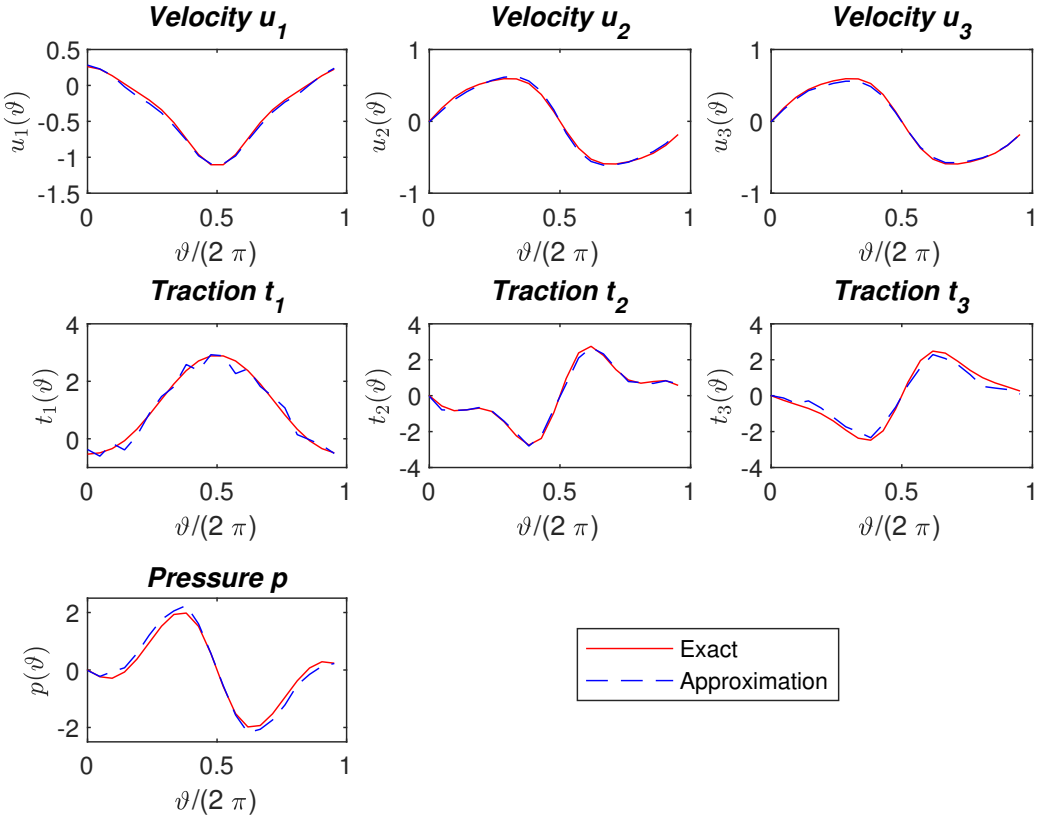

FIGURE 14. Example 3: Results for $\boldsymbol{u}$, $\boldsymbol{t}$ and p along the circle $x^2 + y^2 = 3/4$ on the surface Γ_1 obtained after 500 iterations in case of no noise.

The partial derivatives needed in (A.6) are given by, [24],

$$\frac{\partial G_{ik}}{\partial x_j} = \frac{1}{4\pi\mu\kappa^2 r^5}\left\{(x_j - x_j')\left[3 - \left(3 + 3\kappa r + 2\kappa^2 r^2 + \kappa^3 r^3\right)\mathrm{e}^{-\kappa r}\right]\delta_{ik}\right.$$

$$+ \left((x_k - x_k')\delta_{ij} + (x_i - x_i')\delta_{jk}\right)\left[3 - \left(3 + 3\kappa r + \kappa^2 r^2\right)\mathrm{e}^{-\kappa r}\right]$$

$$\left. + \frac{(x_i - x_i')(x_j - x_j')(x_k - x_k')}{r^2}\left[-15 + \left(15 + 15\kappa r + 6\kappa^2 r^2 + \kappa^3 r^3\right)\mathrm{e}^{-\kappa r}\right]\right\}, \quad i, j, k = 1, 2, 3. \tag{A.7}$$

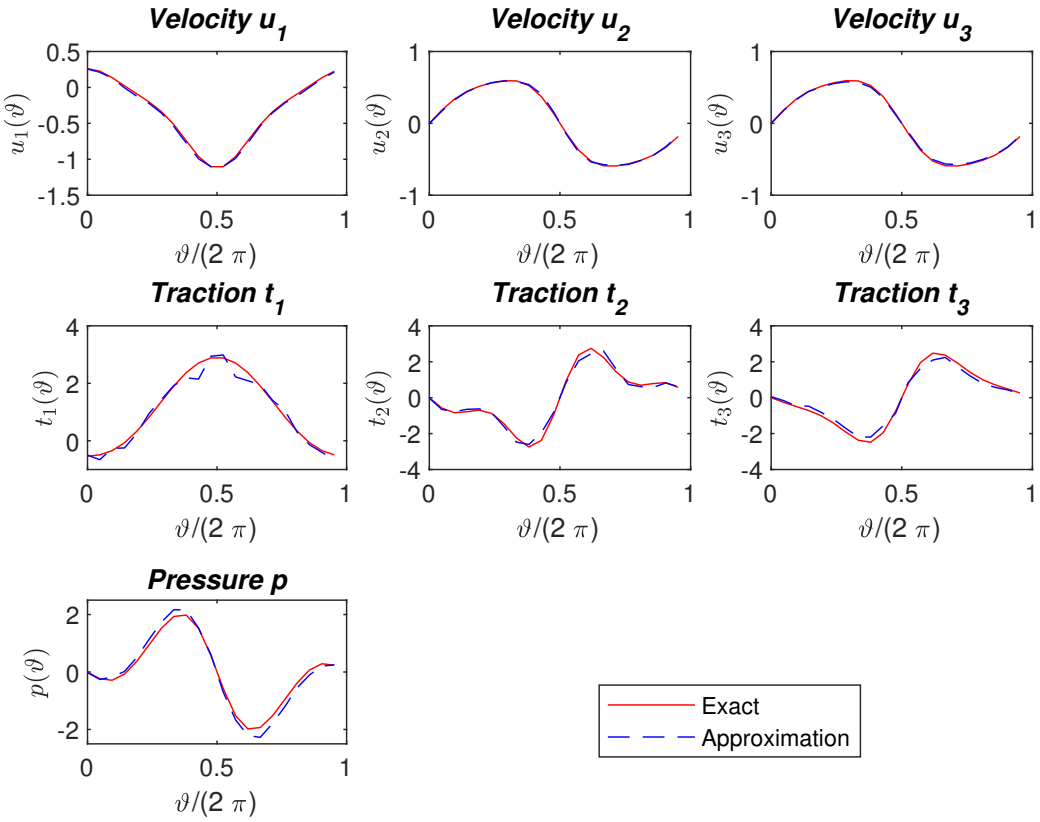

FIGURE 15. Example 3: Results for $\boldsymbol{u}$, $\boldsymbol{t}$ and p along the circle $x^2+y^2=3/4$ on the surface Γ_1, noise p = 1%, obtained after 63 iterations given by the stopping criterion (7.12).

DEPARTMENT OF MATHEMATICS AND STATISTICS, UNIVERSITY OF CYPRUS/ ΠΑΝΕΠΙΣΤΗΜΙΟ ΚΥΠΡΟΥ, P.O.BOX 20537, 1678 NICOSIA/ΛΕΥΚΩΣΙΑ, CYPRUS/ΚΥΠΡΟΣ
Email address, Corresponding author: andreask@ucy.ac.cy

DEPARTMENT OF APPLIED MATHEMATICS, UNIVERSITY OF LEEDS, LEEDS LS2 9JT, UK
Email address: amt5ld@maths.leeds.ac.uk

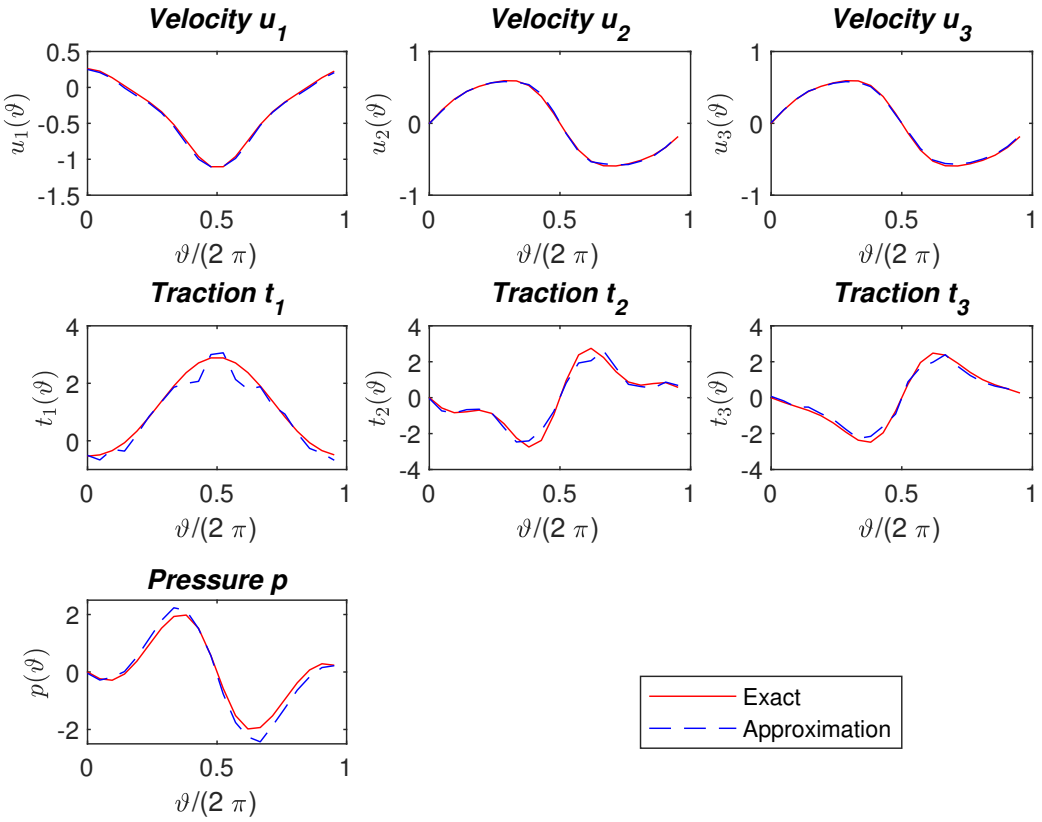

FIGURE 16. Example 3: Results for $\boldsymbol{u}$, $\boldsymbol{t}$ and p along the circle $x^2+y^2=3/4$ on the surface Γ_1, noise p = 3%, obtained after 33 iterations given by the stopping criterion (7.12).

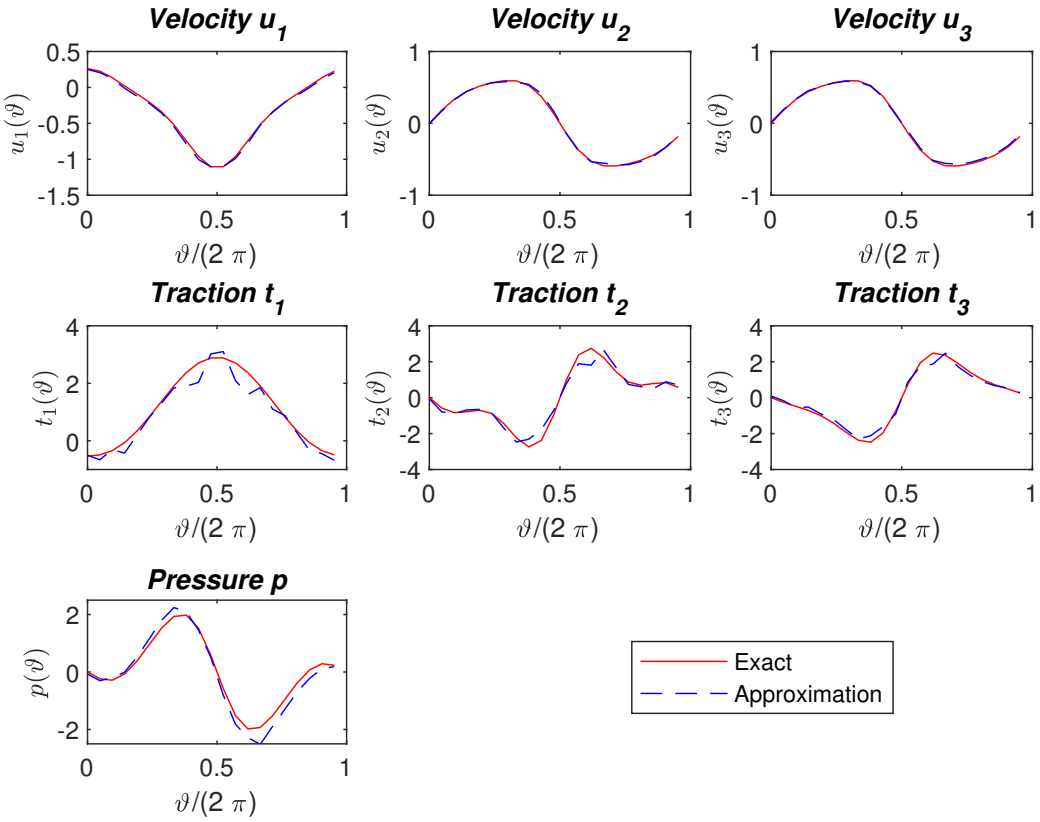

FIGURE 17. Example 3: Results for $\boldsymbol{u}$, $\boldsymbol{t}$ and p along the circle $x^2+y^2=3/4$ on the surface Γ_1, noise p $= 5\%$, obtained after 28 iterations given by the stopping criterion (7.12).